The *Drosophila* chemokine-like Orion bridges phosphatidylserine and Draper in phagocytosis of neurons

Hui Ji[1], Bei Wang[1], Yifan Shen[1], David Labib[1,3], Joyce Lei[1,4], Xinchen Chen[1], Maria Sapar[1,3], Ana Boulanger[2], Jean-Maurice Dura[2] and Chun Han[1,*]

[1]Weill Institute for Cell and Molecular Biology and Department of Molecular Biology and Genetics, Cornell University, Ithaca, NY 14853, USA

[2] IGH, Univ Montpellier, CNRS, Montpellier, France

[3]Current address: The New York Stem Cell Foundation Research Institute, New York, NY 10019, USA

[4]Current address: Tisch MS Research Center of New York, New York, NY 10019, USA

[*]Correspondence: chun.han@cornell.edu

RUNNING TITLE

Orion bridges PS and Drpr in neuronal phagocytosis

ABSTRACT

Phagocytic clearance of degenerating neurons is triggered by “eat-me” signals exposed on the neuronal surface. The conserved neuronal eat-me signal phosphatidylserine (PS) and the engulfment receptor Draper (Drpr) mediate phagocytosis of degenerating neurons in *Drosophila*. However, how PS is recognized by Drpr-expressing phagocytes *in vivo* remains poorly understood. Using multiple models of dendrite degeneration, we show that the *Drosophila* chemokine-like protein Orion can bind to PS and is responsible for detecting PS exposure on neurons; it is supplied cell-non-autonomously to coat PS-exposing dendrites and to mediate interactions between PS and Drpr, thus enabling phagocytosis. As a result, the accumulation of Orion on neurons and on phagocytes produces opposite outcomes by potentiating and suppressing phagocytosis, respectively. Moreover, the Orion dosage is a key determinant of the sensitivity of phagocytes to PS exposed on neurons. Lastly, mutagenesis analyses show that the sequence motifs shared between Orion and human immunomodulatory proteins are important for Orion function. Thus, our results uncover a missing link in PS-mediated phagocytosis in *Drosophila* and imply conserved mechanisms of phagocytosis of neurons.

KEYWORDS

phosphatidylserine, phagocytosis, da neurons, epidermal cells, Orion, Draper, CX_3C, RRY

SIGNIFICANCE STATEMENT

Phagocytes efficiently clear sick or damaged neuronal branches by engulfing them, while leaving healthy branches untouched. How phagocytes recognize degenerating neurites remains poorly understood. Here, we identified a key role for the secreted protein Orion in the detection and engulfment of degenerating neurites in *Drosophila*. Using multiple models of dendrite degeneration, we found that Orion acts as a bridging molecule between the neuronal "eat-me" signal phosphatidylserine and the engulfment receptor Draper on phagocytes, enabling phagocytosis. Our study reveals a missing link in phosphatidylserine-mediated phagocytosis *in vivo*, sheds light on factors determining the sensitivity of phagocytes, and implies the potential for manipulating the detection of neuronal “eat-me” signals in neurodegenerative diseases.

INTRODUCTION

Phagocytosis of apoptotic and degenerative neurons is essential for the development and homeostasis of the nervous system (1, 2). Abnormal phagocytosis is also associated with neuroinflammation and neurodegenerative diseases (3). Neuronal debris is recognized and cleared by resident phagocytes of the nervous system through “eat-me” signals exposed on the neuronal surface. A conserved “eat-me” signal is phosphatidylserine (PS), a negatively charged phospholipid normally kept in the inner leaflet of the plasma membrane by P4-ATPase flippases (4). During neurite degeneration and apoptosis, PS is externalized to the outer surface of neuronal membranes (5-8). Exposed PS dominantly triggers phagocytosis of neurons, as

51 demonstrated by the observation that loss of PS flippases in neurons results in PS exposure and
52 neurodegeneration across species (6, 9, 10). Besides clearing existing neuronal debris, PS-
53 mediated phagocytosis also drives the degeneration of injured neurites and neurons with certain
54 genetic perturbations (6, 11). In the central nervous system (CNS), local PS exposure enables
55 microglia-mediated synaptic elimination (12-14). Thus, the regulation and recognition of
56 neuronal PS exposure are critical for the development and homeostasis of the nervous system.

57 *Drosophila* has been an important model organism for studying neuronal phagocytosis. In
58 *Drosophila*, Draper (Drpr) is the best-known receptor responsible for phagocytosis of neurons
59 (15). As a homolog of the *C. elegans* engulfment receptor CED-1 (16) and the mammalian
60 engulfment receptors Jedi-1 and MEGF10 (17), Drpr is involved in many contexts of neuronal
61 phagocytosis, including the clearance of apoptotic neurons during embryonic development (15,
62 18), axon and dendrite pruning during neuronal remodeling (19, 20), injury-induced neurite
63 degeneration (21, 22), and removal of destabilized boutons at neuromuscular junctions (23).
64 Despite the well-known importance of Drpr in sculping the nervous system, how Drpr recognizes
65 degenerating neurons *in vivo* is still unclear.

66 Recently, the secreted protein Orion was discovered as being required for the
67 developmental pruning and clearance of *Drosophila* mushroom body (MB) axons (24). Orion
68 shares a CX_3C motif with mammalian CX3CL1 (also known as fractalkine), which is required
69 for the elimination of synapses in the mouse barrel cortex (25). CX3CL1 is known as a
70 chemokine because of its ability to direct migration of leukocytes and microglia (26, 27). Thus,
71 Orion represents the first known chemokine-like molecule in *Drosophila* and shares conserved
72 functions with CX3CL1 in the remodeling of the nervous system. However, how Orion and
73 CX3CL1 exactly function in the phagocytosis of neurons is still unknown.

74 In this study, we examined Orion's function in the phagocytosis of *Drosophila* class IV
75 dendritic arborization (C4da) neurons, a well-established *in vivo* model for studying PS-mediated
76 phagocytosis (6, 11, 28). Here we present *in vivo* evidence that the transmembrane engulfment
77 receptor Drpr relies on Orion to sense PS on neurons. Orion is secreted by peripheral non-neural
78 tissues and serves as a non-autonomous permissive factor for phagocytosis of neurons. Orion
79 binds to PS-exposing neurons and is also enriched on phagocytes over-expressing Drpr.
80 Strikingly, a membrane-tethered Orion expressed by neurons dominantly induces phagocytosis
81 even in the absence of PS exposure, while Orion accumulation on the surface of phagocytes
82 makes phagocytes blind to PS-exposing neurons. Importantly, the dosage of Orion determines
83 the sensitivity of phagocytes to neuronal PS exposure. Lastly, we establish that the motifs Orion
84 shares with human chemokines and neutrophil peptides are critical for engulfment of PS-
85 exposing neurons. These findings reveal key mechanisms of PS recognition in *Drosophila* and
86 imply potentially conserved roles of chemokines in PS-mediated phagocytosis of neurons.

87 **RESULTS**

88 ***orion* is required for phagocytosis of dendrites**

89 To determine if *orion* is involved in phagocytosis of degenerating dendrites of da neurons, we
90 first examined phagocytosis of injured C4da dendrites in the *orion*^{1} mutant, which results in a G
91 to D mutation in the C-termini of both Orion protein isoforms (Figure S1A) and abolishes
92 clearance of pruned axons during MB remodeling (24). C4da neurons grow elaborate sensory
93 dendrites on larval epidermal cells (Han et al., 2012), which act as the primary phagocytes during
94 dendrite degeneration and remodeling (Han et al., 2014). Dendrites were severed from the cell
95 body using laser, and engulfment of the injured dendrites was visualized using MApHS, a pH-
96 sensitive dendritic marker consisting of extracellular pHluorin and intracellular tdTom (28).
97 Engulfment was signified by the loss of pHluorin signal due to the drop of pH in early
98 phagosomes (28, 29). Injured dendrites of C4da neurons in the control larvae were completely
99 engulfed by epidermal cells 24 hours (hrs) after injury (AI), as indicated by the loss of pHluorin
100 signals on tdTom-positive dendritic debris dispersed in epidermal cells (Figures 1A-1A", and
101 1D). Because *orion* is located on the X chromosome, we examined both hemizygous male larvae
102 and homozygous female larvae of *orion*^{1}. In contrast to the wildtype (WT), both groups of *orion*^{1}
103 mutants showed little engulfment of injured dendrites by epidermal cells (Figures 1B-1C", and
104 1D), as indicated by the presence of pHluorin signals on tdTom-labeled debris of injured
105 dendrites. The debris remained in the original dendritic patterns, which is another sign of
106 impaired engulfment by epidermal cells. These results suggest that *orion* is required for the
107 engulfment of injured dendrites. Since male and female *orion* mutants exhibited similar degrees
108 of engulfment defects (Figure 1D), we used hemizygous male mutants only in subsequent assays.

109 In addition to phagocytosis after injury, C4da dendrites are all pruned and engulfed by
110 epidermal cells during metamorphosis (28). Consistent with the role of *orion* in axonal pruning
111 of MB neurons (24), we also confirmed that *orion*^{1} exhibits strong defects in the clearance of
112 pruned dendrites of C4da neurons during metamorphosis (Figure S1B-S1D).

113 The engulfment of injured dendrites by epidermal cells is mediated by PS exposure on
114 dendrites (6, 11). To test directly if *orion* is required for PS exposure-induced phagocytosis, we
115 examined a paradigm in which PS exposure was ectopically induced in otherwise healthy
116 neurons using a combination of *CDC50* knockout (KO) and TMEM16F overexpression (OE).
117 *CDC50* encodes a chaperone protein required for the activity of P4-ATPases that keep PS in the
118 inner leaflet of the plasma membrane (30). TMEM16F is a mammalian scramblase that mixes PS
119 between the two leaflets of the plasma membrane (31, 32). Dendrites with *CDC50* KO and
120 TMEM16F OE expose PS and shed membrane in a phagocytosis-dependent manner (6).
121 Whereas these neurons showed reduced dendrite length and elevated debris levels in wandering
122 3rd instar larvae with wildtype *orion* (Figures 1E, 1G, and 1H), *orion*^{1} hemizygous males
123 exhibited almost normal dendritic length and no dendritic debris in epidermal cells (Figures 1F-
124 1H), indicating a lack of engulfment by phagocytes.

125 Because *orion*^{1} carries a missense mutation that may not completely abolish Orion
126 function, we compared its properties to those of *orion*$^{\Delta C}$, a predicted null mutation that lacks all
127 three common C-terminal exons of both *orion* isoforms (Figure S1A) (24). *orion*$^{\Delta C}$ showed

128 similar levels of phagocytosis defects as *orion*^{1} in injury-induced degeneration (Figures S1E-
129 S1E", and 1D), suggesting that *orion*^{1} has lost most, if not all, of its function. Since *orion*
130 encodes two isoforms with different N-terminal sequences (Figure S1A), we next asked if one or
131 both isoforms contribute to phagocytosis. Mutations targeting each of the two *orion* isoforms
132 separately (Figure S1A) showed no phagocytosis defects in injury-induced degeneration (Figure
133 S1F-S1G"), suggesting that OrionA and OrionB isoforms are redundant in the phagocytosis of
134 injured dendrites. These results are consistent with the redundant effects of the same mutations in
135 MB neuron axon pruning (24).

136 **Orion functions cell-non-autonomously**

137 *orion* encodes a secreted protein, raising the question of how it contributes to phagocytosis of
138 dendrites. To determine which tissues express Orion, we generated an *orion* knock-in (KI) allele
139 in which the C-terminus of *orion* is fused in-frame with 4 copies of mNeonGreen2$_{11}$ (mNG2$_{11}$)
140 (33), a V5 tag, a self-cleaving F2A sequence (34), and LexA::VP16 (35) (Figure S2A). This
141 allele, abbreviated as *orion*^{KI}, has several purposes: detection of *orion*-expressing cells by
142 LexA::VP16 transcription activity, detection of endogenous Orion proteins by V5 staining, and
143 visualization of endogenous Orion proteins in a tissue-specific manner by reconstitution of
144 mNG2 fluorescence with tissue-specific expression of mNG2$_{1-10}$ (33).

145 By using *orion*^{KI} with a *LexAop-GFPnls* or a *LexAop-GFP* reporter, we found that *orion*
146 transcripts are expressed in many peripheral tissues in larvae, including epidermal cells,
147 hemocytes, trachea, and the fat body (Figure 2A-2B). However, *orion* transcription is missing in
148 larval da neurons (Figure 2A, inset), even though a weak *orion* transcription activity was later
149 detected in a subset of da neurons at 5-12 hrs after puparium formation (APF) (Figures S2B-
150 S2B"), when some da neurons die and others undergo dendritic pruning (36). In the central
151 nervous system, we found that *orion* was transcribed in most glial cells and in a small subset of
152 neurons at the wandering 3rd instar larval stage (Figure S2C-S2D"). Consistent with a role of
153 *orion* in axonal pruning of MB neurons, *orion* is expressed in Kenyon cells at 8 hrs APF (Figure
154 S2E). Despite the robust LexA::VP16 activity in *orion*^{KI}, Orion proteins appear to be expressed
155 at a low level. Using V5 staining, we could observe only weak Orion signals on the larval
156 epidermis (Figures S2F and S2G). By expressing secreted mNG2$_{1-10}$ in a patch of epidermal cells
157 (in the R16D01 domain), we also detected weak Orion-mNG2 signals in epidermal cells (Figures
158 S2H and S2I).

159 To investigate whether *orion* is required in specific tissues for phagocytosis of injured
160 dendrites, we knocked out *orion* in either neurons or epidermal cells using tissue-specific Cas9s
161 and ubiquitously expressed guide RNAs (gRNAs) (37). As a control, knocking out *orion* with a
162 ubiquitous Cas9 (*Act5C-Cas9*) (38) faithfully replicated the phagocytosis defects of *orion*^{1}
163 (Figures 2C-2E", and 2L), demonstrating the effectiveness of *orion* KO. However, *orion* KO in
164 either da neurons alone (with *SOP-Cas9*; (37)) or in epidermal cells alone (with *shot-Cas9*; (11))
165 did not interfere with the engulfment of injured dendrites (Figures 2F-2G", and 2L).

166 The lack of effect of *orion* KO in da neurons or in epidermal cells suggests that Orion
167 functions cell-non-autonomously. We further tested this idea by asking whether supplying Orion
168 in the extracellular space is sufficient to rescue the impaired engulfment of injured dendrites in
169 *orion* mutants. Extracellular Orion supply was achieved by overexpressing Orion in the fat body,
170 which can efficiently secrete proteins into the hemolymph (6). Because overexpression (OE) of
171 OrionA in the fat body caused early larval lethality, we chose to overexpress a GFP-tagged
172 OrionB (OrionB-GFP) in these rescue experiments. While the debris of injured dendrites
173 remained in the original dendrite patterns in *orion*^{1} hemizygotes (Figure 2H), which indicates a
174 lack of engulfment by epidermal cells, OrionB overexpression in the fat body of *orion*^{1}
175 hemizygotes resulted in even spreading of the debris in the underlying epidermal cells (Figure
176 2I), suggesting successful rescue of engulfment. Similarly, neuronal expression of OrionB-GFP
177 also fully rescued the engulfment defects as measured by the spread of debris (Figure 2J, 2K, and
178 2M).

179 Together, these results indicate that Orion is primarily expressed in non-neural tissues in
180 the periphery and functions cell-non-autonomously for the engulfment of dendrites.

181 **Phosphatidylserine exposure induces Orion binding to the cell surface**

182 To further understand the engulfment defects in *orion* mutants, we examined whether PS
183 exposure on injured dendrites is affected in *orion* mutants. We used fat body-derived Annexin V-
184 mCardinal (AV-mCard) as a PS sensor; it labels injured but not healthy dendrites (6). AV-mCard
185 robustly labeled dendrite fragments in *orion*$^{\Delta C}$ mutant larvae at 24 hrs AI (Figure 3A-3B),
186 suggesting that *orion* LOF does not interfere with PS exposure on injured dendrites.

187 Because Orion is a secreted protein, we asked where Orion is located during engulfment.
188 We observed strong enrichment of fat body-derived OrionB-GFP on injured dendrites at 4-6 hrs
189 AI (Figure 3C-3D, and Movie S1), a timepoint when injured dendrites expose high levels of PS
190 (6). Overexpression of Wld^{S}, a transgene that suppresses fragmentation and PS exposure of
191 injured dendrites when overexpressed in neurons (6, 11), efficiently suppressed OrionB-GFP
192 enrichment on injured dendrites (Figures S3A-S3A", and 3D), indicating that PS exposure may
193 be required for Orion binding to injured dendrites.

194 To test the affinity of Orion for PS-exposing injured dendrites *in vivo*, we examined
195 whether OrionB can compete with the PS sensor AV-mCard for binding to injured dendrites,
196 given that AV binds to PS directly (4). Using long-term time-lapse imaging (39), we found that
197 fat body-derived AV-mCard accumulated on injured dendrites at least 60 minutes before dendrite
198 fragmentation (9/9 movies) (Figures 3E and 3G, and Movie S2). However, when both OrionB-
199 GFP and AV-mCard were co-expressed by the fat body, OrionB-GFP was detected on injured
200 dendrites long before fragmentation (8/8 movies), while AV-mCard did not bind the same
201 injured dendrite in half of the cases (4/8 movies) (Figures 3F and 3G, and Movie S3). In most
202 cases where AV-mCard was observed on injured dendrites (3/4 movies), the labeling only
203 appeared right at the time of dendrite fragmentation (Figure 3G), when PS exposure is at its peak
204 (6). These results suggest that Orion has a higher affinity to injured dendrites compared with AV.

205 To test if neuronal PS exposure is sufficient to induce Orion binding, we ectopically
206 induced dendritic PS exposure by knocking out *CDC50* in neurons (6). Distribution of fat body-
207 derived OrionB-GFP was examined at 96 hrs AEL, a time when *CDC50* KO alone is not yet
208 sufficient to cause membrane loss of dendrites (Figures 3K and 3L). OrionB-GFP showed little
209 binding to wildtype dendrites (Figures 3H-3H", and 3J) but bound robustly to *CDC50* KO
210 dendrites (Figures 3I-3J) at this stage. Interestingly, the presence of OrionB-GFP caused
211 appreciable degeneration of *CDC50* KO dendrites, as indicated by the drastically increased
212 dendrite debris and shortened total dendrite length (Figures 3K and 3L). These results suggest
213 that Orion is recruited to PS-exposing dendrites and OrionB binding on dendrites potentiates
214 epidermal engulfment.

215 The PS-binding C1C2 domain of mouse Lactadherin (LactC1C2) has been used as a PS
216 sensor in multiple systems (5, 6, 40, 41). We previously reported that fat body-derived LactC1C2
217 not only labels degenerating dendrites but also promotes degeneration of *CDC50* KO dendrites
218 (6) (Figures S3B-S3B"). Surprisingly, this degeneration was completely suppressed in the *orion*^{1}
219 hemizygotes (Figures S3C-S3C"), suggesting that the effects of LactC1C2 are mediated by
220 Orion.

221 To further ask if Orion directly interacts with PS *in vitro*, we purified fat body-derived
222 OrionB-GFP protein from larvae and conducted liposome sedimentation assays (42). As positive
223 and negative controls, we also tested AV-GFP and AV(mut)-GFP (6) which carries mutations
224 that abolish AV/PS interactions (40, 43), respectively. As expected, AV-GFP co-precipitated
225 with PS-containing liposomes but not PC-only liposomes (Figures S3E and S3F). In contrast,
226 AV(mut)-GFP did not co-precipitate with either liposomes (Figures S3E and S3G). Surprisingly,
227 about half OrionB-GFP protein in our assay co-precipitated with PC-only liposomes, and
228 liposome-bound OrionB-GFP increased to 62% when PS was added to the liposomes (Figures
229 S3E and S3H). These data suggest that OrionB may have an intrinsic affinity to phospholipid
230 bilayer and that this interaction is enhanced by the presence of PS.

231 *In vivo*, we noticed that OrionB-GFP also binds to the surface of several other peripheral
232 tissues, including epidermal cells, muscles, and trachea (Figures 3H-3H"). The OrionB-GFP
233 binding on epidermal cells was enhanced after we gently pinched the larval body wall (Figures
234 S3D-S3D'), which is expected to mildly disrupt the epidermal cell membrane. To understand
235 how much the binding of OrionB-GFP on epidermal cells depends on PS exposure, we
236 overexpressed ATP8A, an ortholog of the PS-specific flippase TAT-1 (9, 44). Overexpression of
237 ATP8A in da neurons is sufficient to suppress PS exposure and the associated dendrite
238 degeneration caused by genetic perturbations of the NAD^{+} pathway (11). The P4-ATPase
239 chaperone CDC50 was co-expressed with ATP8A in a patch of epidermal cells to facilitate
240 ATP8A trafficking. This manipulation drastically suppressed OrionB-GFP binding on the
241 surface of epidermal cells (Figures 3M-3N), suggesting that Orion binding on epidermal cells is
242 largely mediated by PS exposure.

243 Together, our results suggest that PS exposure induces Orion binding to the cell surface
244 of both neuronal and non-neural cells.

245 **Orion recruits epidermal Drpr to injured dendrites**

246 Because *drpr* is the only other gene known to be required for epidermal engulfment of PS-
247 exposing dendrites (6, 11), we wondered if Orion and Drpr act in the same pathway. We found
248 that *orion*^{1} hemizygous and *drpr* mutant larvae exhibited similar degrees of near complete
249 phagocytosis deficiency in injury-induced dendrite degeneration, as indicated by the portion of
250 unengulfed MApHS-labeled debris (Figures S4A- S4B). We further asked whether removing
251 both *drpr* and *orion* produces stronger phagocytosis defects than the loss of either. We induced
252 whole-body KO of *orion* and *drpr* individually and together. Injured dendrites showed
253 indistinguishable levels of near complete blockage of engulfment in all three genotypes at 24 hrs
254 AI (Figures S4C-S4E), suggesting that *orion* and *drpr* function in the same genetic pathway.

255 To elucidate the epistatic relationship between *orion* and *drpr*, we tested whether the
256 Orion-PS interaction depends on Drpr and whether gain-of-function (GOF) of one gene can
257 compensate for the loss of the other. At 4-5 hrs AI, OrionB-GFP bound to injured dendrites in
258 wildtype and *drpr* null larvae at similar levels (Figure 4A-4B), demonstrating that Orion does not
259 need Drpr for binding to PS. Two observations further suggest that Orion GOF cannot
260 compensate for the loss of *drpr* in engulfment: First, overexpression of Orion in the fat body did
261 not rescue the engulfment of injured dendrites in *drpr* mutants at 24 hrs AI (Figures S4F and
262 4C); and second, the degeneration of *CDC50* KO dendrites induced by OrionB-GFP (Figure 3I-
263 3L) was absent in *drpr* mutants (Figures S4G-S4I). To test the effects of *drpr* GOF in *orion*
264 LOF, we overexpressed Drpr in a patch of epidermal cells in the posterior hemisegment (driven
265 by *hh-Gal4*) of *orion*$^{\Delta C}$ hemizygotes. Interestingly, Drpr OE restored engulfment of injured
266 dendrites, as indicated by the dispersion of dendrite debris specifically in the *hh* domain (Figures
267 4D-4E). These data suggest that phagocytes with overexpressed Drpr does not absolutely need
268 Orion to detect injured dendrites, which could be due to the ability of Drpr extracellular domain
269 to directly interact with PS (18). However, our data also show that, at physiological levels of
270 Drpr, Orion is indispensable for engulfment.

271 To further understand how *orion* LOF affects Drpr, we examined the distribution of Drpr
272 protein by live imaging. For this purpose, we generated a knock-in allele of *drpr* so that the C-
273 terminus of endogenous Drpr is tagged by mNeonGreen (mNG) (45) (Figure S5J). To further
274 boost the Drpr signal, we also made a Drpr-GFP transgene that contains a genomic fragment of
275 the *drpr* locus tagged with GFP at the Drpr C-terminus (Figure S4J). Combining a copy of each
276 of *drpr-mNG* and *drpr-GFP* (referred to as simply *drpr-GFP* because both fluorescent proteins
277 are green), we were able to see robust Drpr recruitment to injured dendrites prior to dendrite
278 fragmentation (Figures 4F-4F" and 4H), which is consistent with how Drpr functions to instruct
279 phagocytosis.. However, this recruitment was abolished in the *orion*^{1} hemizygote, even though
280 injured dendrites showed signs of degeneration, such as thinning and blebbing (Figures 4G-4H).
281 These results suggest that Orion regulates Drpr's response to degenerating dendrites after injury.

282 **Orion mediates the interaction between PS and Drpr**

283 Because Orion interacts with PS and functions genetically upstream of Drpr, we wondered
284 whether Orion mediates PS recognition by interacting with Drpr. We first tested whether Orion
285 could bind to Drpr *in vivo* by expressing Drpr in a patch of epidermal cells (driven by *R16D01-*
286 *Gal4*). Fat body-derived OrionB-GFP was found to accumulate specifically on the surface of
287 these Drpr OE cells in wandering 3rd instar larvae (Figures 5A-5B). Interestingly, some
288 epidermal cells with higher OrionB-GFP enrichment (due to higher Gal4 activities) extruded into
289 neighboring epidermal cells that had low or no OrionB-GFP enrichment (Figures S5A-S5A").
290 We interpret these extrusions as engulfment of high-OrionB cells by low-OrionB cells. To
291 exclude the possibility that OrionB-GFP was recruited by other cell-surface molecules on
292 epidermal cells as a result of Drpr OE, we also tested a truncated Drpr without the intracellular
293 domain (Drpr$^{\Delta Cyto}$), which should be defective in intracellular signaling. Overexpression of
294 Drpr$^{\Delta Cyto}$ also caused drastic OrionB-GFP accumulation on epidermal cells (Figure 5C-5D).
295 These results suggest that OrionB may directly interact with the extracellular domain of Drpr.

296 To further test the hypothesis that Orion mediates the interaction between Drpr and PS,
297 we asked whether expression of an Orion that is permanently tethered to the surface of otherwise
298 wildtype dendrites could bypass the requirement of PS exposure and induce Drpr-dependent
299 phagocytosis. For this purpose, we made an OrionB-CD2-mIFP (mIFP: monomeric infrared
300 fluorescent protein; (46)) transgene in which Orion is located on the extracellular side of the
301 CD2 transmembrane domain (47). As expected, overexpression of OrionB-CD2-mIFP in neurons
302 caused robust dendrite degeneration (Figures 5E-5G, and 5J-5K). We found that this
303 degeneration was completely suppressed by epidermis-specific KO of *drpr* (Figures 5H, and 5J-
304 5K) but was unaffected by suppressing PS exposure in neurons via ATP8A OE (Figures 5I-5K).
305 These data suggest that membrane-tethered Orion is sufficient to induce PS-independent and
306 Drpr-dependent phagocytosis.

307 Meanwhile, if Orion mediates the recognition of PS by Drpr, we predict that excessive
308 Orion on the surface of epidermal cells would interact with Drpr on the same membrane and
309 interfere with the sensing of PS on dendrites. We first tested this idea by overexpressing OrionB-
310 CD2-mIFP in all epidermal cells (Figure 5E). Indeed, this manipulation fully blocked the
311 engulfment of injured dendrites at 25 hrs AI (Figures 5L and 5N). Drpr was robustly detected on
312 the cell membranes of OrionB-CD2-mIFP-expressing cells (Figures S5C and S5D), suggesting
313 that the impaired engulfment was not due to defects in Drpr subcellular localization. We then
314 tested whether accumulation of secreted Orion on the surface of epidermal cells has a similar
315 effect in blocking engulfment. Consistent with the idea that Orion binds PS, *ATP8A* KO in
316 epidermal cells resulted in a drastically increased surface level of OrionB-GFP (Figure 5M').
317 This OrionB-GFP accumulation was associated with phagocytosis deficiency, as indicated by the
318 lack of spread of dendritic debris at 9 hrs AI specifically in the *ATP8A* KO cells (Figure 5M-5N).

319 Together, our results show that interactions between Orion and Drpr from the same
320 versus apposing membranes produce opposite phenotypes (defective versus dominant dendrite
321 engulfment, respectively) and support the idea that Orion functionally bridges PS and Drpr.

322 **The Orion dosage determines the sensitivity of epidermal cells to PS-exposing dendrites**

323 While examining the phenotypes of the *orion*^{1} mutant, we noticed impaired phagocytosis in
324 *orion*^{1}/+ heterozygous larvae: Neurons with *CDC50* KO and TMEM16F OE showed no signs of
325 membrane loss or degeneration in these animals (Figures 6A-6C, 6J-6K), comparable to those in
326 *orion*^{1} hemizygotes. However, the engulfment of injured dendrites was normal in *orion*^{1}/+
327 (Figures S6A-S6B). Considering that *CDC50* KO and TMEM16F OE causes milder PS exposure
328 than does injury (6), these data suggest that removing half the dosage of Orion reduces the
329 sensitivity of epidermal cells to PS exposure on dendrites but does not block phagocytosis when
330 PS exposure is high. To further test if the Orion dosage determines the ability of epidermal cells
331 to sense PS-exposing dendrites, we increased the Orion dosage by adding an *orion* duplication
332 (Dp(1;3)DC496) to the wildtype. The *orion* duplication strongly enhanced the debris level and
333 dendrite loss in a *CDC50* KO background (Figures 6E, 6J-6K), which by itself only causes weak
334 PS exposure (6) and low levels of debris (Figures 6D, 6J-6K). Thus, extra Orion can indeed
335 increase the sensitivity of epidermal cells to neuronal PS.

336 Further supporting this notion, we found that fat body-derived OrionB bound to wildtype
337 dendrites at 120 hrs AEL (Figures S6C) and induced pronounced degeneration (Figures 6F-6G
338 and 6J-6K). This degeneration is PS-dependent because it was completely suppressed by ATP8A
339 OE in neurons (Figure 6H-6I, and 6J-6K). This surprising result demonstrates that, in late larval
340 stages, wildtype dendrites expose low levels of PS that cannot be detected by common PS
341 sensors such as AV and LactC1C2, but can be bound by overexpressed Orion.

342 **CX_3C and RRY motifs are important for Orion function**

343 Orion shares a CX_3C motif with the human chemokine CX3CL1 and an RRY motif with several
344 human neutrophil peptides. The CX_3C motif is required for Orion's function in MB remodeling
345 (24), but the importance of the RRY motif in Orion has not been investigated. To test whether
346 these motifs play any role in PS-mediated dendrite engulfment, we generated *UAS-OrionB-GFP*
347 variants carrying mutations in them (OrionB^{AX3C} and OrionB^{AAY}). We first compared these
348 OrionB-GFP variants in their abilities to potentiate dendrite degeneration of *CDC50* KO
349 neurons, which would be reflected by increased debris level and reduction of dendrite length.
350 Although fat body-derived OrionB^{AX3C} and OrionB^{AAY} both potentiated the debris level of
351 *CDC50* KO neurons (Figures 7A-7D, and 7I), only OrionB^{AX3C}, but not OrionB^{AAY}, caused a
352 weak (21%) dendrite reduction of *CDC50* KO neurons (Figure 7J). In comparison, WT OrionB
353 caused 85% reduction of *CDC50* KO dendrites (Figure 7J). We next tested OrionB-GFP variants
354 in rescuing *orion*$^{\Delta C}$ hemizygotes with the dendrite injury assay. Orion^{AX3C} restored the
355 engulfment of injured dendrites to the same level as WT OrionB-GFP while OrionB^{AAY} only
356 partially restored the engulfment (Figures 7E-7H, and 7I). These results suggest that these
357 mutations impair, but do not abolish, Orion activity.

358 **DISCUSSION**

359 **Orion mediates interactions between PS and Drpr**

360 By triggering phagocytosis, the recognition of PS exposed on neurons is a critical event during
361 neurodegeneration and clearance. Although several studies have implied the involvement of Drpr
362 in this process in *Drosophila* (6, 11, 15, 19-21, 28), how Drpr mediates PS recognition *in vivo* is
363 unclear. In this study, we present several lines of *in vivo* evidence that strongly indicate that the
364 *Drosophila* chemokine-like Orion is a PS-binding bridging molecule that enables Drpr to
365 respond to neuronal PS exposure. First, Orion is required for multiple scenarios of Drpr-
366 dependent phagocytosis of sensory dendrites and functions upstream of Drpr. Second, Orion
367 binds to PS-exposing cell surfaces. We show that Orion binds to neurons and epidermal cells that
368 expose PS as a result of tissue-specific KO of the PS flippase ATP8A. In addition, ATP8A OE,
369 which retains PS in the inner membrane leaflet, eliminates Orion binding on epidermal cells and
370 late-larval dendrites , suggesting that this binding is PS-dependent. Importantly, Orion
371 outcompetes Annexin V for binding to injured dendrites, suggesting that Orion may directly
372 interact with PS *in vivo*. Third, overexpressed Drpr proteins can trap Orion on the cell surface,
373 suggesting that Drpr interacts with Orion *in vivo*. Lastly, when expressed in neurons, membrane-
374 tethered Orion bypasses the requirement for PS in inducing Drpr-dependent engulfment, but
375 when expressed in phagocytes, membrane-tethered Orion blocks PS-induced engulfment. Based
376 on these observations, we propose that Orion functions as a bridging molecule between PS and
377 Drpr.

378 Previously, SIMU, a PS-binding transmembrane protein expressed by *Drosophila*
379 embryonic phagocytes, was proposed to be a bridging molecule (48, 49). Orion and SIMU
380 contribute to phagocytosis through distinct mechanisms. First, SIMU is expressed by phagocytes
381 to allow them to tether apoptotic cells (48), while Orion is secreted from many peripheral tissues
382 and functions as an opsonin to enable phagocytosis. Second, SIMU is a membrane protein that
383 shares homology with Drpr but functions at a different step in apoptotic neuron clearance
384 compared to Drpr (48). In contrast, as a secreted protein, Orion functions at the same step of
385 phagocytosis as Drpr. Therefore, SIMU behaves more like a tethering receptor (49), while Orion
386 is functionally analogous to PS-bridging molecules in other species (41, 50). Although we focus
387 our analyses on the engulfment of somatosensory dendrites, the ubiquitous roles of PS and Drpr
388 in phagocytosis and the broad expression patterns of Orion suggest that Orion may be widely
389 involved in PS-mediated phagocytosis in *Drosophila*. This view is supported by our findings that
390 Orion deposited in the hemolymph can mediate phagocytosis in distant tissues and that the
391 accumulation of Orion on epidermal cells turns these cells into targets of phagocytosis.

392 **The level of Orion modulates phagocyte sensitivity to PS**

393 Although the role of PS exposure in inducing phagocytosis has been well documented (7, 51),
394 what determines the sensitivity of phagocytes to PS is much less understood. In this study, we
395 discovered that the available level of Orion is a determinant of phagocyte sensitivity to PS in
396 *Drosophila*. We show that reducing the dosage of functional Orion by one half makes

397 phagocytes blind to dendrites with moderate levels of PS exposure (i.e. *CDC50* KO +
398 TMEME16F OE neurons), but the reduced Orion does not affect the ability of phagocytes to
399 engulf dendrites that display high levels of PS exposure (i.e. injury). Conversely, an extra copy
400 of the *orion* locus enhances the ability of phagocytes to engulf dendrites that have mild PS
401 exposure (i.e. *CDC50* KO). These results suggest that endogenous Orion is likely expressed at a
402 balanced level to enable the right amount of phagocytosis: Too much Orion may cause
403 unintended phagocytosis of stressed cells that display mild PS exposure, while too little Orion
404 may interfere with efficient clearance of sick cells or structures that are beyond rescue.
405 Consistent with this idea, endogenous Orion is expressed at a low level during larval
406 development (Figure S2G and S2I), but is dramatically upregulated during metamorphosis (24),
407 a time when large-scale tissue remodeling and clearance take place (52).

408 **Orion has distinct roles in neurite maintenance and remodeling**

409 Orion was previously known to be required for axonal pruning and clearance of MB γ Kenyon
410 neurons during metamorphosis (24). In that context, Orion is expressed in the remodeling MB
411 neurons and functions as a "find-me" signal for glia to penetrate the axon bundles and engulf
412 axonal debris. In contrast, in the larval peripheral nervous system (PNS), Orion is supplied by
413 many non-neural tissues and functions as a permissive signal for phagocytosis of sick or broken
414 dendrites. This distinction is likely due to two differences between the larval PNS and the
415 remodeling CNS. First, in the PNS, the dendrites of da neurons are exposed to the hemolymph
416 and are readily accessible to Orion that is secreted from other tissues, whereas in the CNS, the
417 axons are more tightly packed and may be harder for extrinsic Orion to access. Neuron-derived
418 Orion would thus be more effective than extrinsic Orion for promoting phagocytosis in the CNS.
419 Intriguingly, we detected Orion expression in a small number of neurons in the larval ventral
420 nerve cord (VNC). It will be interesting to find out whether these neurons are particularly subject
421 to degeneration. Second, compared to the larval PNS where degenerative events are rare, the
422 nervous system undergoing metamorphosis has a much greater demand for phagocytosis.
423 Turning on Orion expression in neurons may thus be required for efficient clearance of all
424 pruned neurites. Consistent with this idea, we detected Orion expression also in a subset of da
425 neurons during metamorphosis.

426 **Orion possesses unique properties compared to other PS-binding molecules**

427 Fluorescent PS probes based on AV and Lact are widely used to visualize PS exposure in cell
428 culture and live animals and have been crucial for many discoveries in PS biology (6, 40, 41, 53,
429 54). LactC1C2 is known to have a higher affinity to PS than AV (55-57). We previously
430 observed additional differences between these two proteins. Compared to LactC1C2, which coats
431 the dendrite surface well, AV tends to traffic to endocytic vesicles inside PS-exposing dendrites,
432 consistent with the ability of the AV complex to induce endocytosis upon PS-binding (58, 59).
433 Importantly, unlike AV, which does not alter the kinetics of neurite degeneration, LactC1C2
434 binding to PS-exposing dendrites potentiates Drpr-dependent degeneration (6). This latter
435 observation previously led us to hypothesize that LactC1C2 may contain unknown sequences

436 that interact with Drpr (6). In this study, we show that the effect of LactC1C2 in exacerbating
437 dendrite degeneration depends on Orion, suggesting instead that LactC1C2 may indirectly
438 promote phagocyte/dendrite interactions by enhancing Orion function. One possible mechanism
439 is that LactC1C2 binding on the plasma membrane further disrupts the membrane and causes
440 more PS exposure that can subsequently be detected by endogenous Orion.

441 Compared to AV and LactC1C2, Orion displays unique lipid binding properties. Our *in*
442 *vivo* evidence suggests that Orion may have a higher affinity for PS than AV, as Orion efficiently
443 outcompetes AV in binding to injured dendrites. In addition, overexpressed Orion binds to
444 healthy epidermal cells and dendrites (albeit the latter only in wandering 3rd instar larvae), while
445 AV and LactC1C2 do not (6). Although our *in vitro* evidence suggests that Orion may have an
446 intrinsic affinity for phospholipid bilayers, *in vivo* Orion-binding to epidermal cells and WT
447 dendrites largely depends on PS exposure. One possibility is that other endogenous factors
448 modify Orion-lipid interactions and make Orion more specific to PS *in vivo*.

449 The surprising finding that overexpressed Orion binds to peripheral tissues and dendrites
450 suggest that these cells may expose PS under physiological conditions, perhaps at a level too low
451 to detect by AV and LactC1C2. Thus, low levels of PS exposure may be much more prevalent *in*
452 *vivo* than previously thought. Intriguingly, binding of overexpressed Orion induces degeneration
453 of wildtype dendrites but does not cause obvious phagocytosis of other non-neural tissues,
454 suggesting that neurons may be more vulnerable to PS-induced phagocytosis than other cell
455 types.

456 **Functional conservation between Orion and human immunomodulatory proteins**

457 Recently, many human chemokines were found to bind to PS exposed on apoptotic vesicles and
458 serve as "find-me" signals to attract phagocytes (60). Orion shares the CX_3C motif with the
459 mammalian chemokine CXC3L1 and has also three glycosaminoglycan (GAG) putative binding
460 sequences, a hallmark of chemokine activity (61). Even though direct binding to PS has not been
461 demonstrated for CXC3L1, this chemokine is required for microglia-mediated synapse
462 elimination after whisker lesioning (25), a process likely involving PS exposure (62). In addition,
463 Orion contains a RRY motif commonly found in human neutrophil peptides, small antimicrobial
464 peptides important for innate immunity (63). We found that both CX_3C and RRY motifs are
465 important for Orion function in mediating phagocytosis of neurons. Although Orion does not
466 show global sequence homologies to mammalian immunomodulatory proteins, its interaction
467 partner Drpr has mammalian homologs that are involved in phagocytosis of neurons through
468 unknown mechanisms (17). Thus, the common features between Orion and human proteins
469 indicate that a functional conservation may exist between PS-sensing mechanisms in insects and
470 humans.

471 **METHODS**

472 **Fly strains**

473 The details of fly strains used in this study are listed in Table S1 (Key Resource Table). For
474 labeling of C4da neurons, we used *ppk-MApHS*, *ppk-CD4-tdTom*, and *ppk-Gal4 UAS-CD4-*
475 *tdTom*. For labeling of all da neurons, we used *21-7-Gal4 UAS-CD4-tdTom*. For labeling PS
476 exposure on dendrites, we used *dcg-Gal4 UAS-AnnexinV-mCard* and *dcg-Gal4 UAS-GFP-*
477 *LactC1C2*. For visualizing OrionB labeling on cell surface, we used *dcg-Gal4 UAS-OrionB-*
478 *GFP*, *Dcg-LexA LexAop-OrionB-GFP*, and *R16A03-LexA LexAop-OrionB-GFP*. We generated
479 *dcg-LexA* by converting the Gal4 in *dcg-Gal4* into LexAGAD. The conversion process will be
480 published elsewhere.

481 See Supplemental Methods for details of molecular cloning and transgenic flies,
482 generation of KI flies, CRISPR-TRiM, live imaging, immunohistochemistry, protein
483 purification, liposome sedimentation assay, image analysis and quantification, and statistical
484 analysis. See Table S2 for gRNA target sequences.

485 **DATA SHARING PLANS**

486 All study data are included in the article and/or Supplemental Methods. Constructs and fly
487 strains will be available upon request.

488 **ACKNOWLEDGMENTS**

489 We thank Larry Zipursky, Loren Looger, Xinhua Lin, BACPAC Resources Center, *Drosophila*
490 Genomics Resource Center (DGRC), the National Cancer Institute (NCI), and Addgene for
491 plasmids; Marc Freeman and Bloomington Stock Center for fly stocks; Cornell BRC Imaging
492 facility for access to microscopes (funded by NIH grant S10OD018516); Cornell CSCU for
493 advice on statistics; lab members of Chris Fromme, Jeremy Baskin, and Yuxin Mao for technical
494 assistance and advice on biochemistry; Shaogeng Tang for experimental tests; Mike Goldberg
495 for critical reading and suggestions on the manuscript. This work was supported by NIH grants
496 (R01NS099125 and R21OD023824) awarded to C.H., and by ARC grant (PJA 20151203422)
497 and FRM grant (DEQ20160334870) awarded to J.-M.D.

498 **DECLARATION OF INTEREST**

499 The authors declare no competing interests.

500 **REFERENCE**

501 1. Galloway DA, Phillips AEM, Owen DRJ, & Moore CS (2019) Phagocytosis in the Brain:
502 Homeostasis and Disease. *Front Immunol* 10:790.
503 2. Frost JL & Schafer DP (2016) Microglia: Architects of the Developing Nervous System.
504 *Trends Cell Biol* 26(8):587-597.
505 3. Salter MW & Stevens B (2017) Microglia emerge as central players in brain disease. *Nat*
506 *Med* 23(9):1018-1027.
507 4. Leventis PA & Grinstein S (2010) The distribution and function of phosphatidylserine in
508 cellular membranes. *Annu Rev Biophys* 39:407-427.
509 5. Shacham-Silverberg V*, et al.* (2018) Phosphatidylserine is a marker for axonal debris
510 engulfment but its exposure can be decoupled from degeneration. *Cell Death Dis*
511 9(11):1116.
512 6. Sapar ML*, et al.* (2018) Phosphatidylserine Externalization Results from and Causes
513 Neurite Degeneration in Drosophila. *Cell Rep* 24(9):2273-2286.
514 7. Nagata S (2018) Apoptosis and Clearance of Apoptotic Cells. *Annu Rev Immunol* 36:489-
515 517.
516 8. Sievers C, Platt N, Perry VH, Coleman MP, & Conforti L (2003) Neurites undergoing
517 Wallerian degeneration show an apoptotic-like process with Annexin V positive staining
518 and loss of mitochondrial membrane potential. *Neurosci Res* 46(2):161-169.
519 9. Darland-Ransom M*, et al.* (2008) Role of C. elegans TAT-1 protein in maintaining plasma
520 membrane phosphatidylserine asymmetry. *Science* 320(5875):528-531.
521 10. Zhu X*, et al.* (2012) Mutations in a P-type ATPase gene cause axonal degeneration. *PLoS*
522 *Genet* 8(8):e1002853.
523 11. Ji H, Sapar ML, Sarkar A, Wang B, & Han C (2022) Phagocytosis and self-destruction
524 break down dendrites of Drosophila sensory neurons at distinct steps of
525 Wallerian degeneration. *Proceedings of the National Academy of Sciences*
526 119(4):e2111818119.
527 12. Li T*, et al.* (2020) A splicing isoform of GPR56 mediates microglial synaptic refinement
528 via phosphatidylserine binding. *EMBO J* 39(16):e104136.
529 13. Scott-Hewitt N*, et al.* (2020) Local externalization of phosphatidylserine mediates
530 developmental synaptic pruning by microglia. *EMBO J* 39(16):e105380.
531 14. Park J*, et al.* (2021) Microglial MERTK eliminates phosphatidylserine-displaying
532 inhibitory post-synapses. *EMBO J* 40(15):e107121.
533 15. Freeman MR, Delrow J, Kim J, Johnson E, & Doe CQ (2003) Unwrapping glial biology:
534 Gcm target genes regulating glial development, diversification, and function. *Neuron*
535 38(4):567-580.
536 16. Zhou Z, Hartwieg E, & Horvitz HR (2001) CED-1 is a transmembrane receptor that
537 mediates cell corpse engulfment in C. elegans. *Cell* 104(1):43-56.
538 17. Wu HH*, et al.* (2009) Glial precursors clear sensory neuron corpses during development
539 via Jedi-1, an engulfment receptor. *Nat Neurosci* 12(12):1534-1541.
540 18. Tung TT*, et al.* (2013) Phosphatidylserine recognition and induction of apoptotic cell
541 clearance by Drosophila engulfment receptor Draper. *J Biochem* 153(5):483-491.

542 19. Awasaki T*, et al.* (2006) Essential role of the apoptotic cell engulfment genes draper and
543 ced-6 in programmed axon pruning during Drosophila metamorphosis. *Neuron*
544 50(6):855-867.
545 20. Williams DW, Kondo S, Krzyzanowska A, Hiromi Y, & Truman JW (2006) Local caspase
546 activity directs engulfment of dendrites during pruning. *Nat Neurosci* 9(10):1234-1236.
547 21. MacDonald JM*, et al.* (2006) The Drosophila cell corpse engulfment receptor Draper
548 mediates glial clearance of severed axons. *Neuron* 50(6):869-881.
549 22. Tao J & Rolls MM (2011) Dendrites have a rapid program of injury-induced degeneration
550 that is molecularly distinct from developmental pruning. *J Neurosci* 31(14):5398-5405.
551 23. Fuentes-Medel Y*, et al.* (2009) Glia and muscle sculpt neuromuscular arbors by engulfing
552 destabilized synaptic boutons and shed presynaptic debris. *PLoS Biol* 7(8):e1000184.
553 24. Boulanger A*, et al.* (2021) Axonal chemokine-like Orion induces astrocyte infiltration and
554 engulfment during mushroom body neuronal remodeling. *Nat Commun* 12(1):1849.
555 25. Gunner G*, et al.* (2019) Sensory lesioning induces microglial synapse elimination via
556 ADAM10 and fractalkine signaling. *Nat Neurosci* 22(7):1075-1088.
557 26. Bazan JF*, et al.* (1997) A new class of membrane-bound chemokine with a CX3C motif.
558 *Nature* 385(6617):640-644.
559 27. Maciejewski-Lenoir D, Chen S, Feng L, Maki R, & Bacon KB (1999) Characterization of
560 fractalkine in rat brain cells: migratory and activation signals for CX3CR-1-expressing
561 microglia. *J Immunol* 163(3):1628-1635.
562 28. Han C*, et al.* (2014) Epidermal cells are the primary phagocytes in the fragmentation and
563 clearance of degenerating dendrites in Drosophila. *Neuron* 81(3):544-560.
564 29. Botelho RJ & Grinstein S (2011) Phagocytosis. *Curr Biol* 21(14):R533-538.
565 30. Segawa K & Nagata S (2015) An Apoptotic 'Eat Me' Signal: Phosphatidylserine Exposure.
566 *Trends Cell Biol* 25(11):639-650.
567 31. Nagata S, Suzuki J, Segawa K, & Fujii T (2016) Exposure of phosphatidylserine on the cell
568 surface. *Cell Death Differ* 23(6):952-961.
569 32. Suzuki J, Umeda M, Sims PJ, & Nagata S (2010) Calcium-dependent phospholipid
570 scrambling by TMEM16F. *Nature* 468(7325):834-838.
571 33. Feng S*, et al.* (2017) Improved split fluorescent proteins for endogenous protein
572 labeling. *Nat Commun* 8(1):370.
573 34. Szymczak AL*, et al.* (2004) Correction of multi-gene deficiency in vivo using a single 'self-
574 cleaving' 2A peptide-based retroviral vector. *Nat Biotechnol* 22(5):589-594.
575 35. Chen Y*, et al.* (2014) Cell-type-specific labeling of synapses in vivo through synaptic
576 tagging with recombination. *Neuron* 81(2):280-293.
577 36. Williams DW & Truman JW (2005) Cellular mechanisms of dendrite pruning in
578 Drosophila: insights from in vivo time-lapse of remodeling dendritic arborizing sensory
579 neurons. *Development* 132(16):3631-3642.
580 37. Poe AR*, et al.* (2019) Robust CRISPR/Cas9-Mediated Tissue-Specific Mutagenesis Reveals
581 Gene Redundancy and Perdurance in Drosophila. *Genetics* 211(2):459-472.
582 38. Port F, Chen HM, Lee T, & Bullock SL (2014) Optimized CRISPR/Cas tools for efficient
583 germline and somatic genome engineering in Drosophila. *Proc Natl Acad Sci U S A*
584 111(29):E2967-2976.

585 39. Ji H & Han C (2020) LarvaSPA, A Method for Mounting Drosophila Larva for Long-Term
586 Time-Lapse Imaging. *J Vis Exp* (156).
587 40. Mapes J*, et al.* (2012) CED-1, CED-7, and TTR-52 regulate surface phosphatidylserine
588 expression on apoptotic and phagocytic cells. *Curr Biol* 22(14):1267-1275.
589 41. Hanayama R*, et al.* (2002) Identification of a factor that links apoptotic cells to
590 phagocytes. *Nature* 417(6885):182-187.
591 42. Shami Shah A*, et al.* (2019) PLEKHA4/kramer Attenuates Dishevelled Ubiquitination to
592 Modulate Wnt and Planar Cell Polarity Signaling. *Cell Rep* 27(7):2157-2170 e2158.
593 43. Dubois T*, et al.* (1998) Annexin V inhibits protein kinase C activity via a mechanism of
594 phospholipid sequestration. *Biochem J* 330 (Pt 3)(Pt 3):1277-1282.
595 44. Wehman AM, Poggioli C, Schweinsberg P, Grant BD, & Nance J (2011) The P4-ATPase
596 TAT-5 inhibits the budding of extracellular vesicles in C. elegans embryos. *Curr Biol*
597 21(23):1951-1959.
598 45. Shaner NC*, et al.* (2013) A bright monomeric green fluorescent protein derived from
599 Branchiostoma lanceolatum. *Nat Methods* 10(5):407-409.
600 46. Yu D*, et al.* (2015) A naturally monomeric infrared fluorescent protein for protein
601 labeling in vivo. *Nat Methods* 12(8):763-765.
602 47. Yan D, Wu Y, Feng Y, Lin SC, & Lin X (2009) The core protein of glypican Dally-like
603 determines its biphasic activity in wingless morphogen signaling. *Dev Cell* 17(4):470-481.
604 48. Kurant E, Axelrod S, Leaman D, & Gaul U (2008) Six-microns-under acts upstream of
605 Draper in the glial phagocytosis of apoptotic neurons. *Cell* 133(3):498-509.
606 49. Shklyar B, Levy-Adam F, Mishnaevski K, & Kurant E (2013) Caspase activity is required for
607 engulfment of apoptotic cells. *Mol Cell Biol* 33(16):3191-3201.
608 50. Wang X*, et al.* (2010) Caenorhabditis elegans transthyretin-like protein TTR-52 mediates
609 recognition of apoptotic cells by the CED-1 phagocyte receptor. *Nat Cell Biol* 12(7):655-
610 664.
611 51. Lemke G (2019) How macrophages deal with death. *Nat Rev Immunol* 19(9):539-549.
612 52. Williams DW & Truman JW (2005) Remodeling dendrites during insect metamorphosis. *J*
613 *Neurobiol* 64(1):24-33.
614 53. Andersen MH, Graversen H, Fedosov SN, Petersen TE, & Rasmussen JT (2000) Functional
615 analyses of two cellular binding domains of bovine lactadherin. *Biochemistry*
616 39(20):6200-6206.
617 54. Koopman G*, et al.* (1994) Annexin V for flow cytometric detection of phosphatidylserine
618 expression on B cells undergoing apoptosis. *Blood* 84(5):1415-1420.
619 55. Shi J, Heegaard CW, Rasmussen JT, & Gilbert GE (2004) Lactadherin binds selectively to
620 membranes containing phosphatidyl-L-serine and increased curvature. *Biochim Biophys*
621 *Acta* 1667(1):82-90.
622 56. Tait JF & Gibson D (1992) Phospholipid binding of annexin V: effects of calcium and
623 membrane phosphatidylserine content. *Arch Biochem Biophys* 298(1):187-191.
624 57. Andree HA*, et al.* (1990) Binding of vascular anticoagulant alpha (VAC alpha) to planar
625 phospholipid bilayers. *J Biol Chem* 265(9):4923-4928.
626 58. Oling F*, et al.* (2000) Structure of membrane-bound annexin A5 trimers: a hybrid cryo-
627 EM - X-ray crystallography study. *J Mol Biol* 304(4):561-573.

59. Kenis H*, et al.* (2004) Cell surface-expressed phosphatidylserine and annexin A5 open a novel portal of cell entry. *J Biol Chem* 279(50):52623-52629.
60. Pontejo SM & Murphy PM (2021) Chemokines act as phosphatidylserine-bound "find-me" signals in apoptotic cell clearance. *PLoS Biol* 19(5):e3001259.
61. Monneau Y, Arenzana-Seisdedos F, & Lortat-Jacob H (2016) The sweet spot: how GAGs help chemokines guide migrating cells. *J Leukoc Biol* 99(6):935-953.
62. Faust TE, Gunner G, & Schafer DP (2021) Mechanisms governing activity-dependent synaptic pruning in the developing mammalian CNS. *Nat Rev Neurosci* 22(11):657-673.
63. Klotman ME & Chang TL (2006) Defensins in innate antiviral immunity. *Nat Rev Immunol* 6(6):447-456.

663 **FIGURES AND FIGURE LEGENDS**

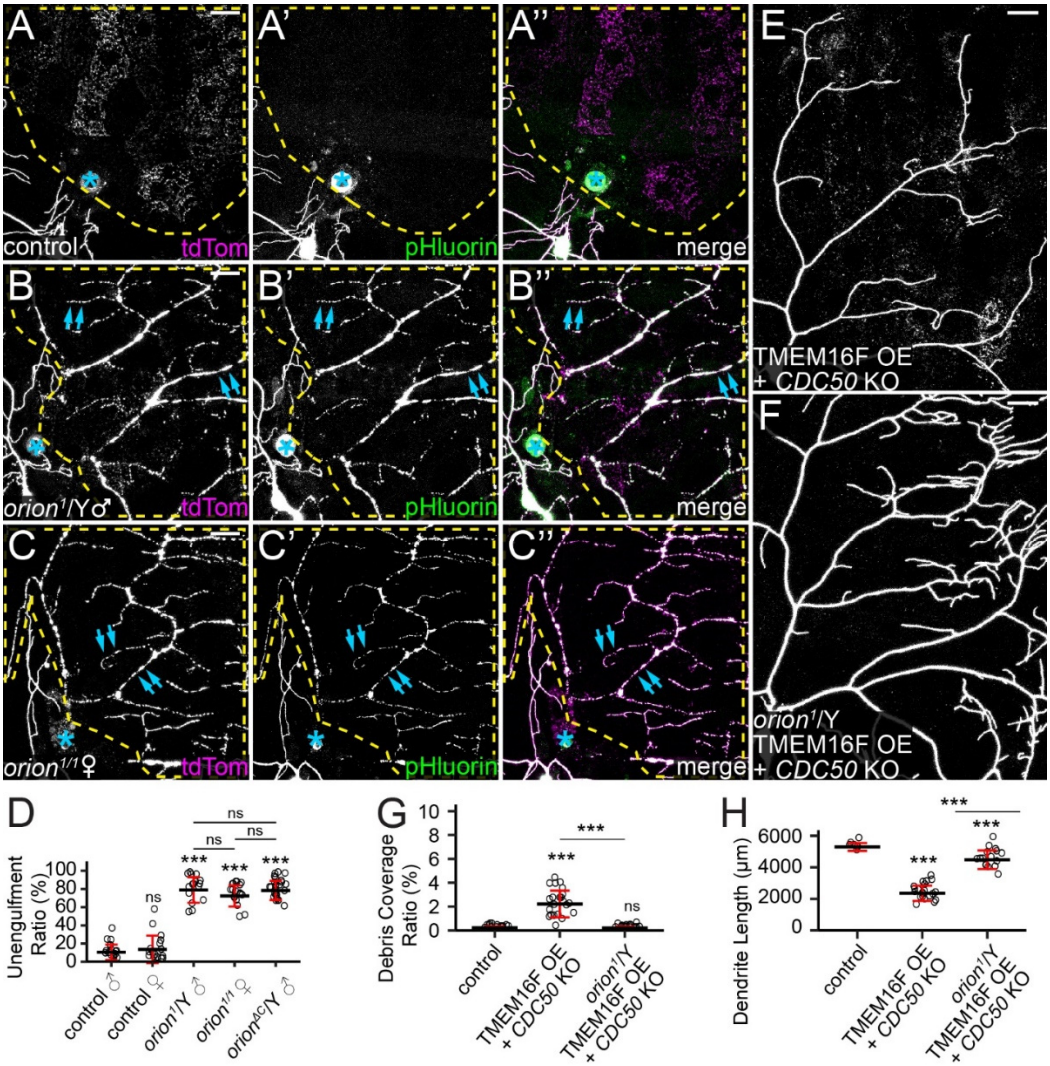

664

665 **Figure 1: *orion* is required for phagocytosis of dendrites in multiple dendrite degeneration paradigms**
666 (A-C") Partial dendritic fields of ddaC neurons in control (A-A"), *orion*^{1} hemizygous (B-B"), and *orion*^{1}
667 homozygous (C-C") larvae at 22-24 hrs after injury (AI). Yellow dash outlines: territories originally covered by
668 injured dendrites; blue asterisks: injury sites; blue arrows: injured but unengulfed dendrite fragments.
669 (D) Quantification of unengulfment ratio of injured dendrites (pHluorin-positive debris area/tdTom-positive debris
670 area). n = number of neurons and N = number of animals: control males (n = 18, N = 10); control females (n = 16, N
671 = 9); *orion*^{1}/Y (n = 16, N = 8); *orion*$^{1/1}$ (n = 18, N = 9); *orion*$^{\Delta C}$/Y (n = 25, N = 12). One-way ANOVA and Tukey's
672 test.
673 (E and F) Partial dendritic fields of TMEM16F OE + *CDC50* KO neurons in the wildtype background (E) and *orion*^{1}
674 hemizygous background (F).
675 (G and H) Quantification of debris coverage ratio (percentage of debris area normalized by dendrite area) (G) and
676 dendrite length (H) at 140 hrs after egg laying (AEL). n = number of neurons and N = number of animals: control (n
677 = 14, N = 7); TMEM16F OE + *CDC50* KO (n = 22, N = 11); TMEM16F OE + *CDC50* KO in *orion*^{1}/Y (n = 16, N =
678 8). For (G), Kruskal-Wallis (One-way ANOVA on ranks) and Dunn's test, p-values adjusted with the Benjamini-
679 Hochberg method; for (H), One-way ANOVA and Tukey's test.
680 In all image panels, neurons were labeled by *ppk-MApHS*. Scale bars, 25 µm. For all quantifications, ***p≤0.001;
681 n.s., not significant. The significance level above each genotype is for comparison with the control. Black bar, mean;
682 red bar, SD. See also Figure S1.

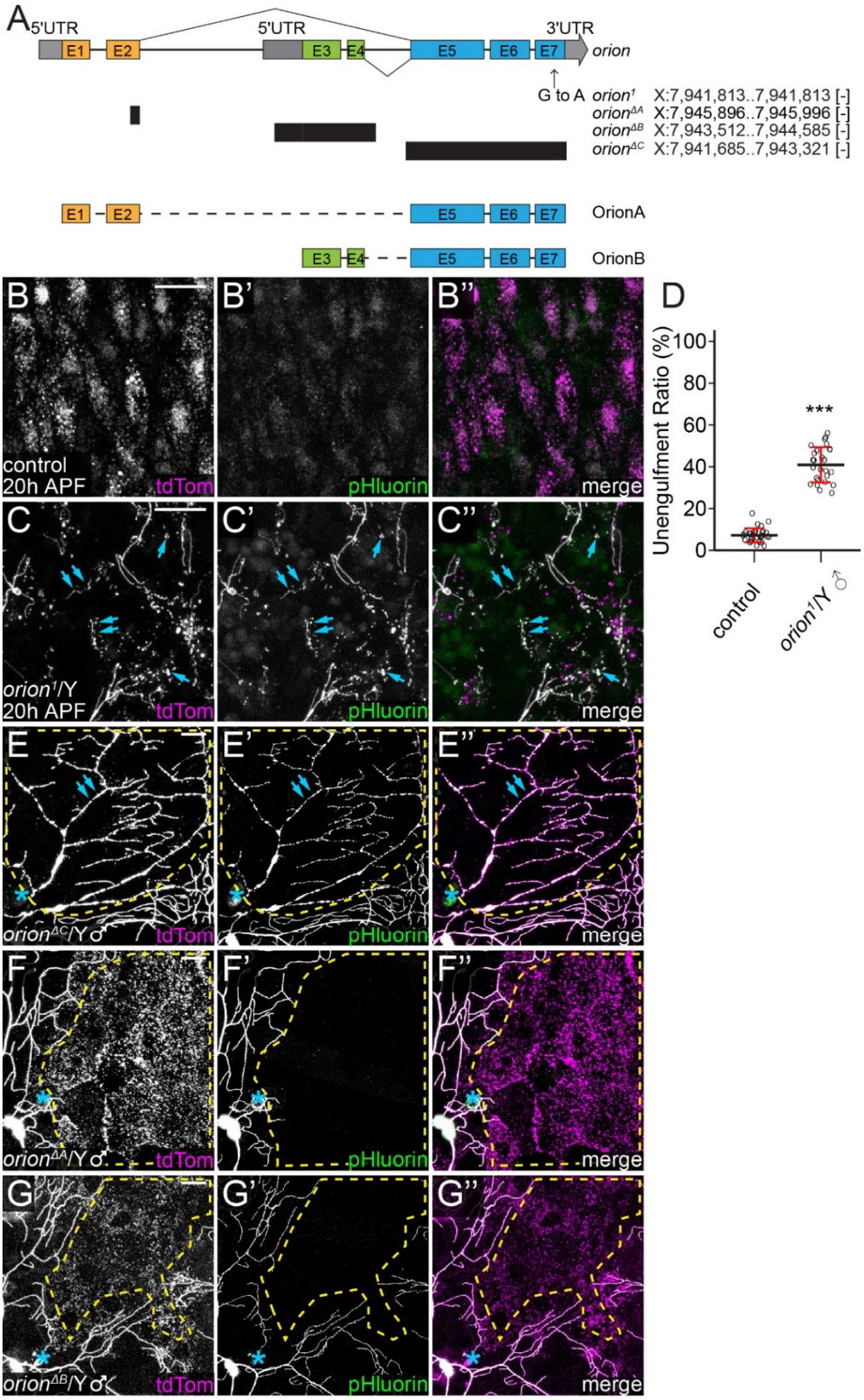

Figure S1: *orion* mutant alleles and engulfment phenotypes

686 (A) Schematic representation of the *orion* locus in the wildtype and in four different *orion* alleles (*orion*^{1}, *orion*$^{\Delta A}$,
687 *orion*$^{\Delta B}$ and *orion*$^{\Delta C}$). Black bars indicate deleted regions. The two mRNA splicing isoforms of *orion* are also
688 indicated. The *orion* gene annotation is based on Release 6 reference genome assembly.
689 (B-C") Partial dendritic fields of ddaC neurons at 20 hrs after puparium formation (APF) in wildtype (B-B") and
690 *orion*^{1} hemizygous (C-C") pupae. Blue arrows: unengulfed dendrite fragments.
691 (D) Quantification of unengulfment ratio of pruned dendrites (area of pHluorin-positive debris/area of tdTom-
692 positive debris) at 19-21 hrs APF. n = number of neurons and N = number of animals: control (n = 30, N = 12);
693 *orion*^{1} hemizygotes (n = 26, N = 9). Welch's t-test; ***$p \leq 0.001$; black bar, mean; red bars, SD.
694 (E-E") Partial dendritic field of a ddaC neuron in *orion*$^{\Delta C}$ hemizygotes at 23 hrs AI. Blue arrows: injured but
695 unengulfed dendrite fragments.
696 (F-G") Partial dendritic fields of ddaC neurons in *orion*$^{\Delta A}$ hemizygotes (G-G"), and *orion*$^{\Delta B}$ hemizygotes (G-G") at
697 23-24 hrs AI.
698 In all image panels, neurons were labeled by *ppk-MApHS*. Scale bars, 25 μm. In (E-G"), yellow dash outlines:
699 territories originally covered by injured dendrites; blue asterisks: injury sites.

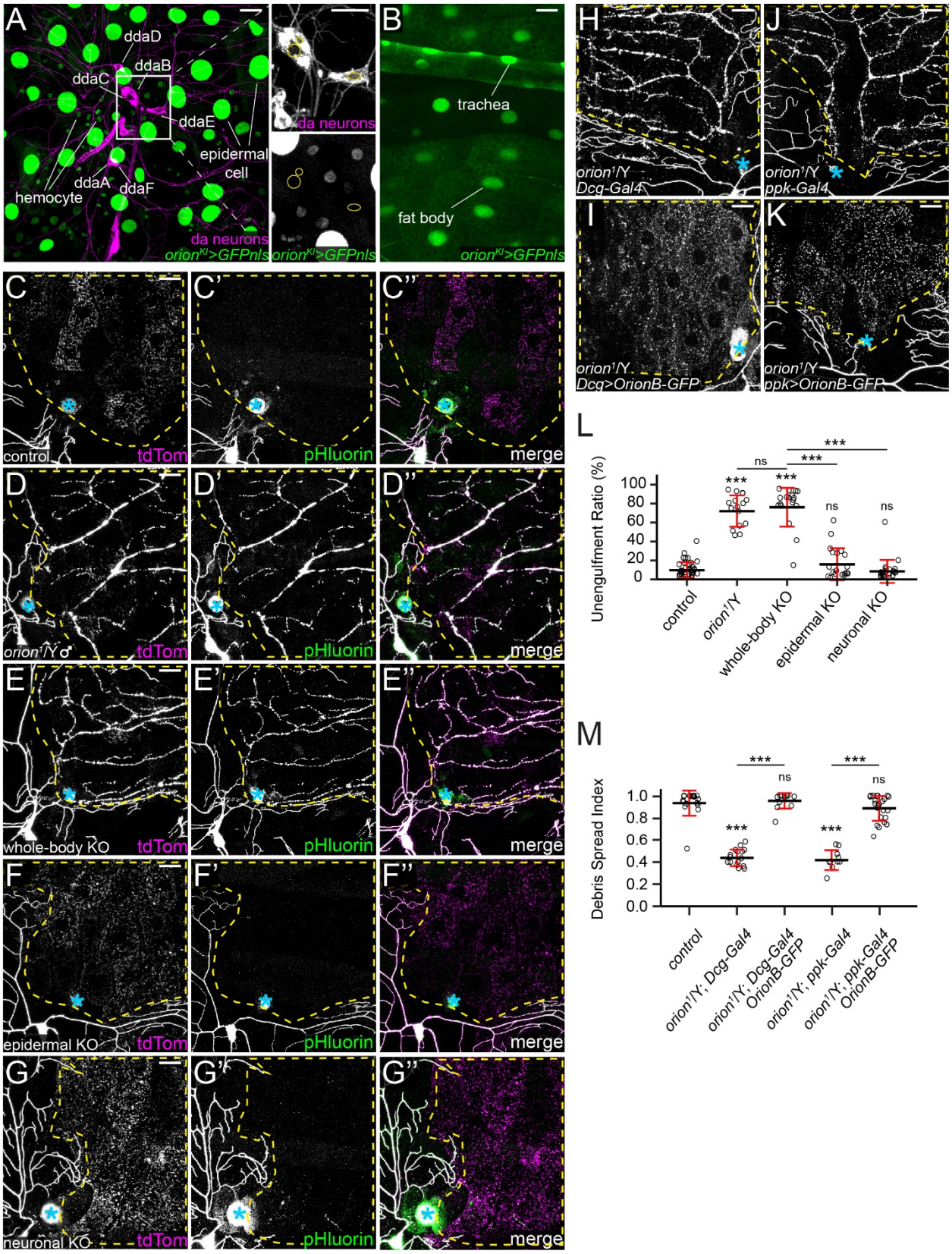

Figure 2: Orion functions cell-non-autonomously

(A-B) GFPnls expression driven by *orion-LexA* (*orion*^{KI}) in epidermal cells, hemocytes (A), trachea, and fat body (B), but not in da neurons (A, insets). Yellow circles indicate nuclei of ddaB, ddaC, and ddaE neurons (A). Scale bars, 25 µm (A), 10 µm (A insets), and 50 µm (B).
(C-G") Partial dendritic fields of neurons in control (C-C", same images as Figure 1A-1A"), *orion*^{1} hemizygotes (D-D", same images as Figure 1B-1B" for clarity), whole-body *orion* KO (E-E"), epidermal *orion* KO (F-F"), and neuronal *orion* KO (G-G") at 22-24 hrs AI.
(H-K) Partial dendritic fields of ddaC neurons in *orion*^{1} hemizygotes with fat body Gal4 (H), with OrionB-GFP OE in the fat body (I), with neuron Gal4 (J), and with OrionB-GFP OE in neurons (K) at 22-24 hrs AI.
(L) Quantification of unengulfment ratio of injured dendrites. n = number of neurons and N = number of animals: control and *orion*^{1}/Y (same dataset as in Figure 1D); whole-body *orion* KO (n = 18, N = 10); epidermal *orion* KO (n = 19, N = 11); neuronal *orion* KO (n = 21, N = 11). One-way ANOVA and Tukey's test.
(M) Quantification of debris spread index of injured dendrites (area ratio of all 15 pixel x 15 pixel squares that contained dendrite debris in the region of interest). n = number of neurons and N = number of animals: *orion*^{1}/Y (n = 18, N = 10); *Dcg-Gal4* in *orion*^{1}/Y (n = 16, N = 9); *Dcg>OrionB-GFP* in *orion*^{1}/Y (n = 13, N = 7), *ppk-Gal4* in *orion*^{1}/Y (n = 10, N = 6); *ppk>OrionB-GFP* in *orion*^{1}/Y (n = 24, N = 12). One-way ANOVA and Tukey's test.
Neurons were labeled by *21-7>UAS-CD4-tdTom* (A-B), *ppk-MApHS* (C-G"), *ppk-CD4-tdTom* (H, I), and *ppk>CD4-tdTom* (J, K). In (C-K), yellow dash outlines: territories originally covered by injured dendrites; blue asterisks: injury sites; scale bars, 25 µm. For all quantifications, ***$p \leq 0.001$; n.s., not significant. The significance level above each genotype is for comparison with the control. Black bar, mean; red bar, SD. See also Figure S2.

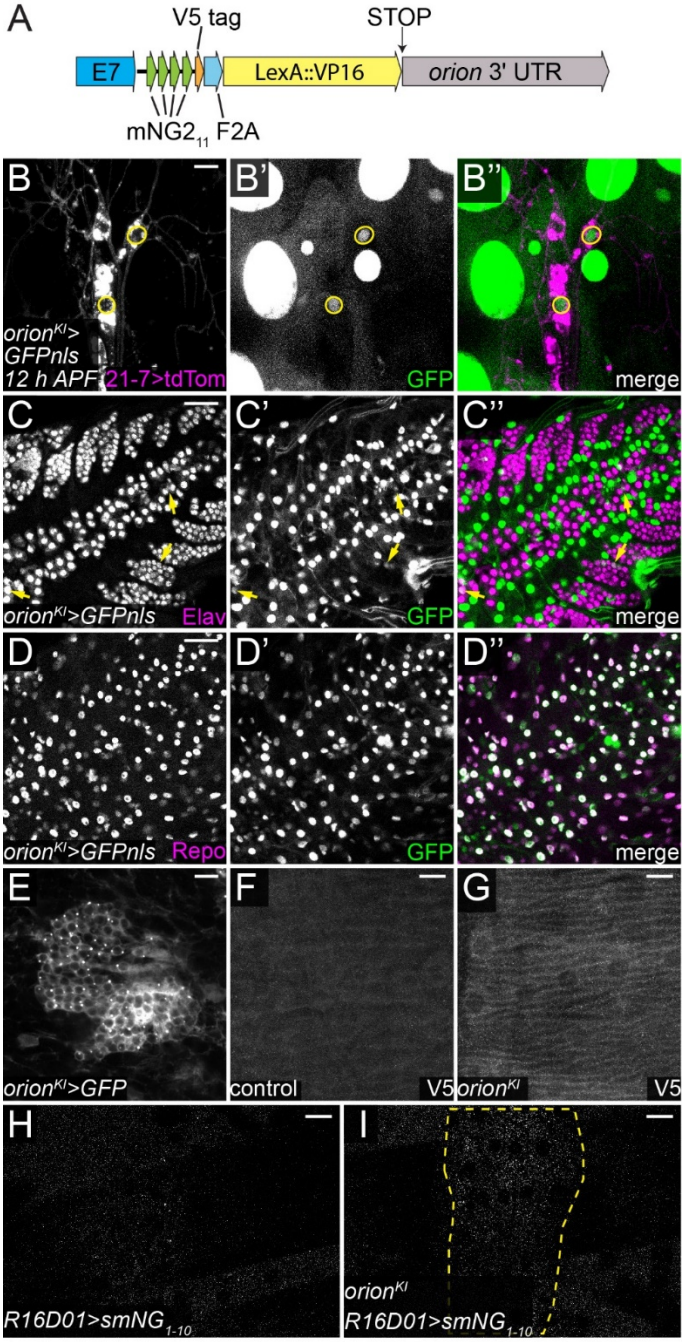

Figure S2: Orion functions cell-non-autonomously

(A) Schematic representation of the *orion^{KI}* allele.

(B-B") GFPnls expression driven by *orion-LexA* in ddaC and ddaE neurons at 12 hrs APF. Yellow circles indicate nuclei of ddaC and ddaE neurons. Neurons were labeled by *21-7-Gal4>CD4-tdTom*.

(C-D") GFPnls expression driven by *orion-LexA* in the larval ventral nerve cord (VNC). Nuclei of neurons are labeled by Elav staining (C-C"); glial nuclei are labeled by Repo staining (D-D"). Yellow arrows (C-C"): a small number of neurons expressing *orion*.

(E) GFP expression driven by *orion-LexA* in the mushroom body Kenyon cells at 8 hrs APF.

(F-G) V5 staining of larval body walls in the wildtype control (w^{1118}) (F) and *orion^{KI}* (G).

(H-I) Signals of reconstituted mNG in control (H) and *orion^{KI}* (I) epidermal cells. Secreted mNG$_{1-10}$ (smNG$_{1-10}$) was expressed in patches of epidermal cells (outlined in H) driven by *R16D01-Gal4*.

Scale bars, 10 µm (B and E) and 25 µm (C-D" and F-I).

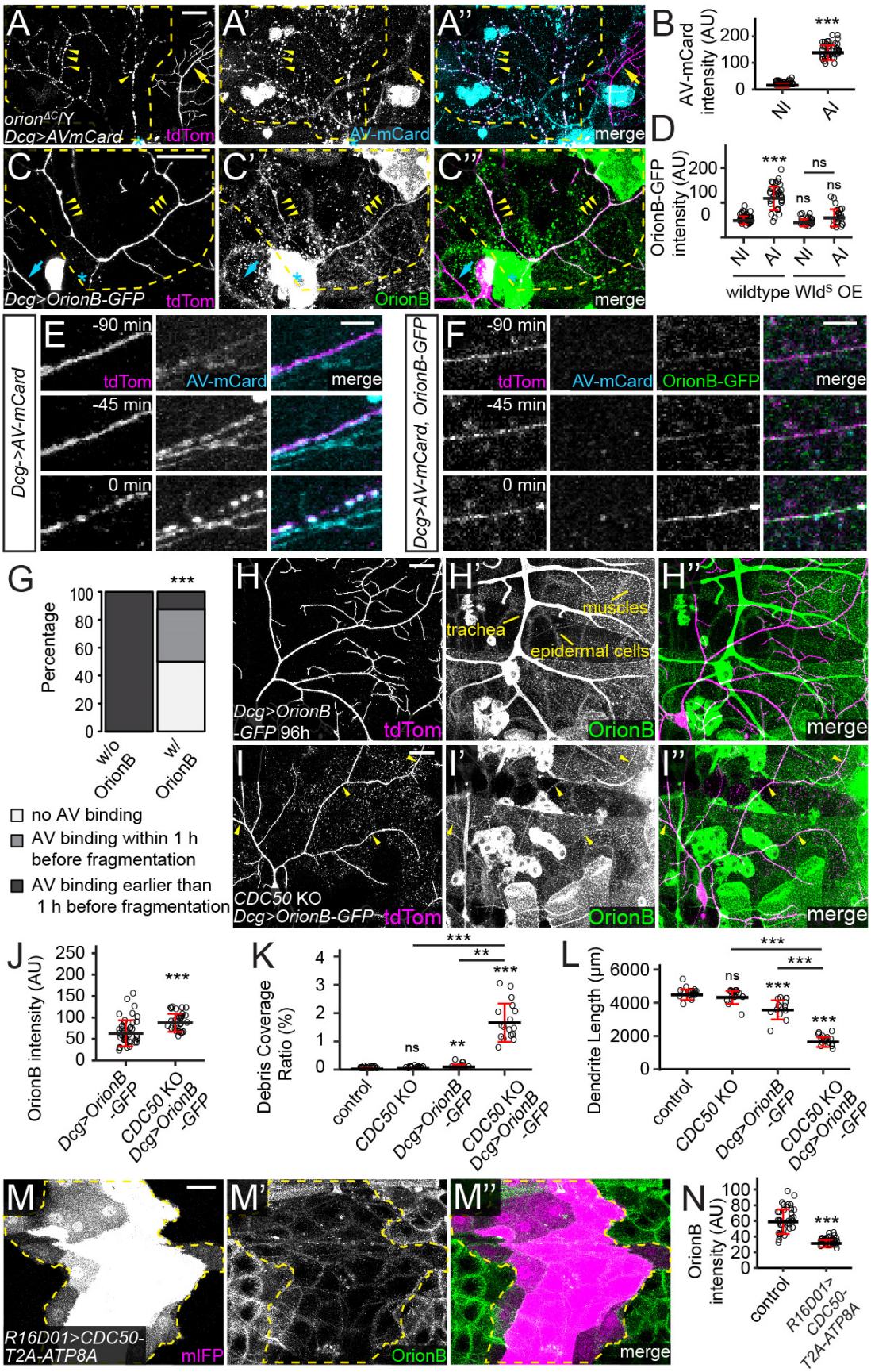
A
orionΔC/Y
Dcg>AVmCard
tdTom
A'
AV-mCard
A''
merge
B
AV-mCard intensity (AU)
200
100
0
***
NI
AI
C
Dcg>OrionB-GFP
tdTom
C'
OrionB
C''
merge
D
OrionB-GFP intensity (AU)
200
100
0
***
ns
ns
ns
NI
AI
NI
AI
wildtype
WldS OE
Dcg->AV-mCard
E
-90 min
tdTom
AV-mCard
merge
-45 min
0 min
Dcg>AV-mCard, OrionB-GFP
F
-90 min
tdTom
AV-mCard
OrionB-GFP
merge
-45 min
0 min
G
Percentage
100
80
60
40
20
0
***
w/o OrionB
w/ OrionB
no AV binding
AV binding within 1 h before fragmentation
AV binding earlier than 1 h before fragmentation
H
Dcg>OrionB -GFP 96h
tdTom
H'
trachea
muscles
epidermal cells
OrionB
H''
merge
I
CDC50 KO
Dcg>OrionB-GFP
tdTom
I'
OrionB
I''
merge
J
OrionB intensity (AU)
250
200
150
100
50
0
***
Dcg>OrionB -GFP
CDC50 KO Dcg>OrionB -GFP
K
Debris Coverage Ratio (%)
4
3
2
1
0
***
**
***
ns
**
control
CDC50 KO
Dcg>OrionB -GFP
CDC50 KO Dcg>OrionB -GFP
L
Dendrite Length (µm)
6000
4000
2000
0
***
ns
***
***
***
control
CDC50 KO
Dcg>OrionB -GFP
CDC50 KO Dcg>OrionB -GFP
M
R16D01>CDC50-T2A-ATP8A
mIFP
M'
OrionB
M''
merge
N
OrionB intensity (AU)
100
80
60
40
20
0
***
control
R16D01> CDC50-T2A-ATP8A

734

735 **Figure 3: PS exposure induces Orion binding to the cell surface**
736 (A-A") Labeling of injured dendrites of a ddaC neuron by AV-mCard at 23 hrs AI in *orion*$^{\Delta C}$ hemizygous larvae.
737 Yellow arrowheads: injured dendrites with AV-mCard labeling; yellow arrows: uninjured dendrites lacking AV-
738 mCard labeling.
739 (B) Quantification of AV-mCard binding on dendrites. AV-mCard intensities were measured on both uninjured (NI)
740 and injured (AI) dendrites. n = number of measurements and N = number of animals: NI (n = 39, N = 8); AI (n = 39,
741 N = 8). Welch's t-test.
742 (C-C") Labeling of injured dendrites of a ddaC neuron by Orion-GFP at 6 hrs AI in wildtype larvae. Yellow
743 arrowheads: injured dendrites with OrionB-GFP labeling.
744 (D) Quantification of Orion-GFP binding on dendrites of wildtype and Wld^{S} OE neurons. n = number of
745 measurements and N = number of animals: wildtype NI (n = 39, N = 10); wildtype AI (n = 36, N = 10); Wld^{S} OE NI
746 (n = 22, N = 6); Wld^{S} OE AI (n = 23, N = 6). Kruskal-Wallis (One-way ANOVA on ranks) and Dunn's test, p-
747 values adjusted with the Benjamini-Hochberg method.
748 (E-F) Time series of injured dendrites of ddaC neurons from 90 min before fragmentation to the moment of
749 fragmentation, with only AV-mCard expressed (E) or both OrionB-GFP and AV-mCard co-expressed (F) by the fat
750 body. Time stamps are relative to the frame of dendrite fragmentation.
751 (G) Percentages of injured dendrites showing no AV binding, AV binding within 1 hr before fragmentation, AV
752 binding earlier than 1 hr before fragmentation. n = number of measurements and N = number of animals: w/o
753 OrionB OE (n = 9, N = 5); w/ OrionB OE (n = 8, N = 3). Fisher's exact test.
754 (H-I") Distribution of fat body-derived OrionB-GFP with wildtype (H-H") and *CDC50* KO (I-I") dendrites at 96 hrs
755 AEL. Peripheral tissues showing OrionB-binding are labeled in (H'). Yellow arrowheads indicate OrionB-binding
756 on *CDC50* KO dendrites (I-I").
757 (J) Quantification of OrionB-GFP binding on wildtype and *CDC50* KO dendrites. n = number of measurements:
758 *Dcg>OrionB-GFP* (n = 41, N = 7); *CDC50* KO + *Dcg>OrionB-GFP* (n = 29, N = 6). Welch's t-test.
759 (K-L) Quantification of debris coverage ratio (K) and dendrite length (L) at 96 hrs AEL. n = number of neurons and
760 N = number of animals: control (n = 17, N = 9); *CDC50* KO (n = 15, N = 8); *Dcg>OrionB-GFP* (n = 13, N = 8);
761 *CDC50* KO + *Dcg>OrionB-GFP* (n = 17, N = 9). For (K), Kruskal-Wallis (One-way ANOVA on ranks) and
762 Dunn's test, p-values adjusted with the Benjamini-Hochberg method; for (L), one-way ANOVA and Tukey's test.
763 (M-M") OrionB-GFP binding on epidermal cells that expressed *CDC50-T2A-ATP8A*. Yellow dash outlines:
764 *CDC50-T2A-ATP8A* overexpressing region.
765 (N) Quantification of OrionB-GFP binding on wildtype epidermal cells and *CDC50-T2A-ATP8A* OE epidermal
766 cells. n = number of measurements and N = number of animals: control (n = 36, N = 9); *R16D01>CDC50-T2A-*
767 *ATP8A* (n = 36, N = 9). Welch's t-test.
768 In (A-A") and (C-C"), yellow dash outlines: territories originally covered by injured dendrites; blue asterisks: injury
769 sites. Neurons were labeled by *ppk-MApHS* (A-A" and E-E"), and *ppk-CD4-tdTom* (C-C", F-F" and H-I"). Scale
770 bars, 25 µm (A-A", C-C", H-I"), 5 µm (E-F), and 50 µm (M-M"). For all quantifications, **p≤0.01, ***p≤0.001;
771 n.s., not significant. The significance level above each genotype is for comparison with the control. Black bar, mean;
772 red bar, SD. See also Movie S1-S3 and Figure S3.
773 **Movie S1**: OrionB-GFP labels degenerating dendrites after injury, related to Figure 3. Time-lapse movie of laser-
774 injured ddaC dendrites from 2.5 to 11 hrs AI, showing OrionB-GFP labeling on injured dendrites. The dendrite
775 arbor on the bottom right was injured while the ones at the top were not. The mobile cells in the OrionB-GFP
776 channel are hemocytes. Time stamp is relative to the first frame.
777 **Movie S2**: AV-mCard labels injured dendrites before dendrite fragmentation, related to Figure 3. Time-lapse movie
778 of laser-injured ddaC dendrites from 2.5 to 5 hrs AI, showing AV-mCard labeling on injured dendrites as early as 2
779 hrs before fragmentation. The AV-mCard signals that do not colocalize with tdTom signals indicate AV-mCard
780 labeling on injured dendrites of other types of neurons. Time stamp is relative to the frame of dendrite
781 fragmentation.
782 **Movie S3**: AV-mCard fails to label injured dendrites when OrionB-GFP is co-expressed, related to Figure 3. Time-
783 lapse movie of laser-injured ddaC dendrites from 1 to 3 hrs AI showing OrionB-GFP labeling but not AV-mCard
784 labeling on injured dendrites before fragmentation. Time stamp is relative to the frame of dendrite fragmentation.

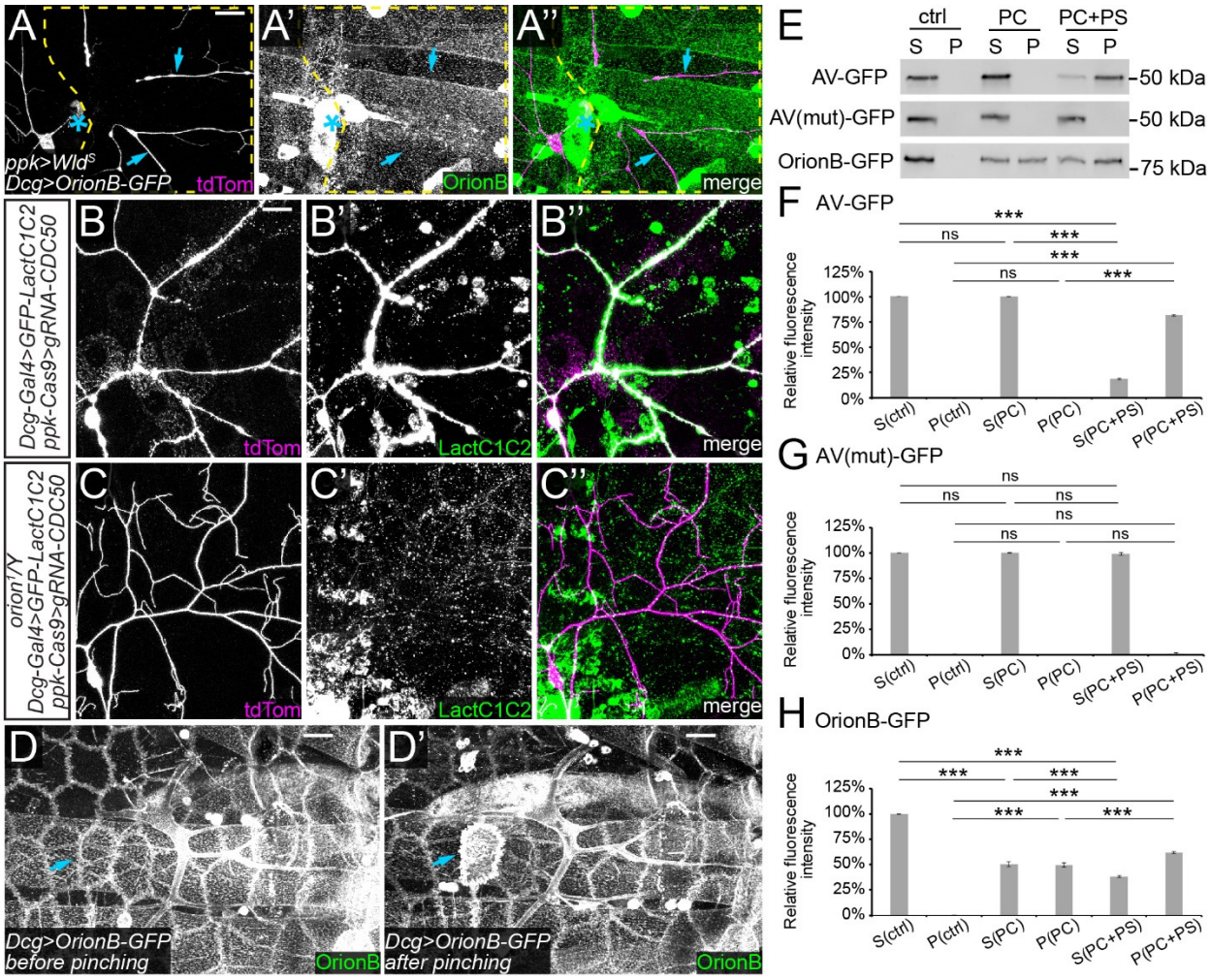

Figure S3: PS exposure induces Orion binding to the cell surface

(A-A") Lack of OrionB-GFP labeling on injured dendrites of a ddaC neuron with Wld^S OE at 6 hrs AI. Yellow dash outlines: territories originally covered by injured dendrites; blue asterisks: injury sites; blue arrows: injured dendrites lacking OrionB-GFP labeling.

(B-C") *CDC50* KO neurons in the presence of fat body-derived GFP-LactC1C2 in control (B-B") and *orion*^{1} hemizygous (C-C") larvae.

(D-D') OrionB-GFP binding on epidermal cells before (D) and after (D') gentle pinching. Blue arrows indicate enhanced OrionB binding.

(E) Western blot of liposome sedimentation assay. Ctrl, control without liposomes; PC, PC-only liposomes; PC+PS, liposomes containing 20% PS; S, supernatant; P, pellet.

(F-H) Quantification of signal intensity of AV-GFP (F), AVmut-GFP (G), and OrionB-GFP (H) in the western blot of liposome sedimentation assay. n=3.

Neurons were labeled by *ppk-CD4-tdTom* (A-C"). In all image panels, scale bars, 25 µm.

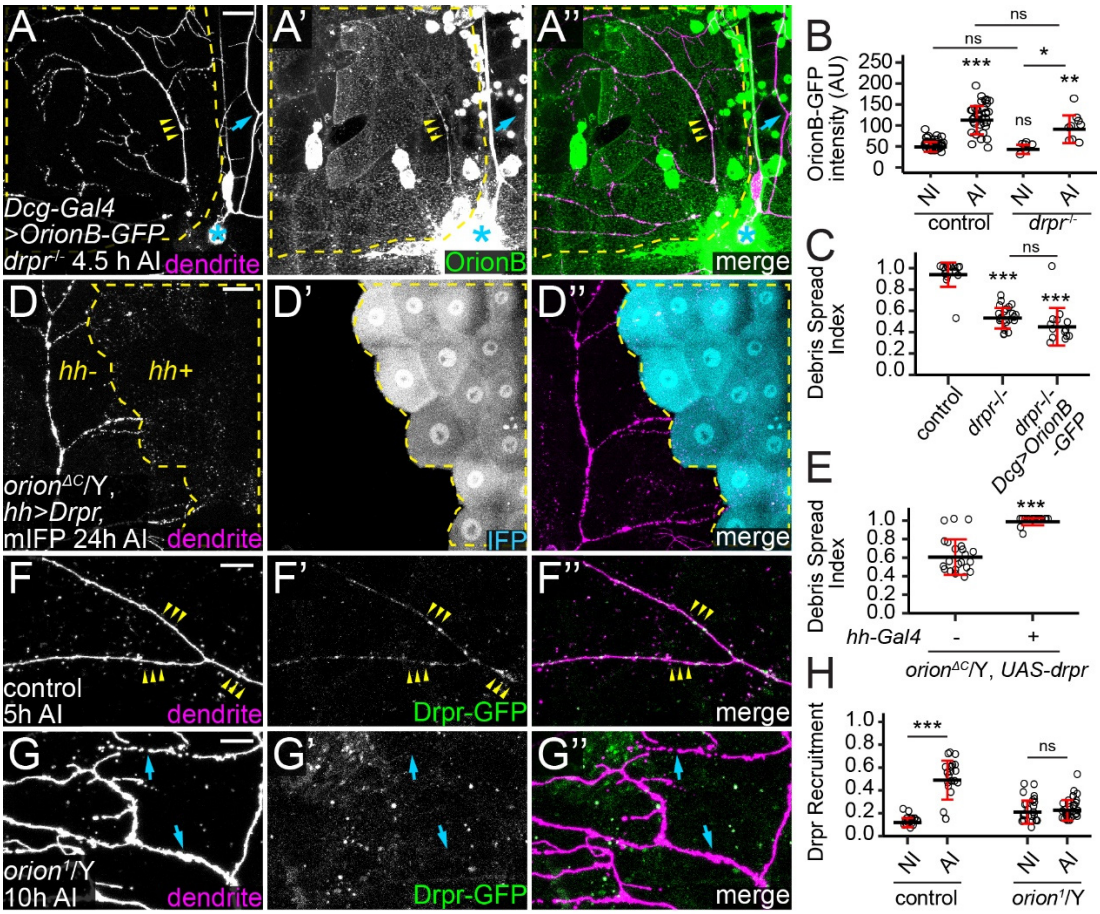

Figure 4: Orion recruits epidermal Drpr to injured dendrites

(A-A") Labeling of injured dendrites of a ddaC neuron by OrionB-GFP in *drpr*$^{-/-}$ at 4.5 hrs AI. Yellow arrowheads: injured dendrites with OrionB-GFP labeling; blue arrows: uninjured dendrites lacking OrionB-GFP binding.

(B) Quantification of Orion-GFP binding on dendrites in the wildtype and the *drpr*$^{-/-}$ larvae. n = number of measurements and N = number of animals: wildtype NI and wildtype AI (same dataset as in Figure 3D); *drpr*$^{-/-}$ NI (n = 6, N = 2); *drpr*$^{-/-}$ AI (n = 9, N = 3). Kruskal-Wallis (One-way ANOVA on ranks) and Dunn's test, p-values adjusted with the Benjamini-Hochberg method.

(C) Quantification of debris spread index of injured dendrites at 22-24 hrs AI. n = number of neurons and N = number of animals: control (same dataset as in 2M); *drpr*$^{-/-}$ (n = 23, N = 10); *drpr*$^{-/-}$ + *Dcg>OrionB-GFP* (n = 14, N = 7). One-way ANOVA and Tukey's test.

(D-D") Engulfment of injured dendrites in an *orion*$^{\Delta C}$ hemizygous larva with Drpr overexpressed in the *hh* domain. Yellow dash outlines: *hh>Drpr, mIFP* region.

(E) Quantification of debris spread index of injured dendrites at 22-24 hrs AI in region without Drpr OE and region with Drpr OE in *orion*$^{\Delta C}$*/Y*. n = number of neurons and N = number of animals: region without Drpr OE (n = 22, N = 12); and region with Drpr OE (n = 24, N = 12). Welch's t-test.

(F-F") Distribution of Drpr-GFP in the presence of injured dendrites in control at 5 hrs AI (F-F") and in *orion*^{1}*/Y* at 10 hrs AI (G-G"). Yellow arrowheads (F-F"): injured dendrites with Drpr-GFP recruitment; bule arrowheads (G-G"): injured dendrites lacking Drpr-GFP recruitment.

(H) Quantification of Drpr-GFP recruitment (Drpr-GFP-positive area on dendrites/total dendrite area). n = measurements: control NI (n = 20, N = 12); control AI (n = 21, N = 12); *orion*^{1}*/Y* NI (n = 27, N = 8); *orion*^{1}*/Y* AI (n = 31, N = 8). Welch's t-test.

For all image panels, neurons were labeled by *ppk-CD4-tdTom*. Yellow dash outlines: territories originally covered by injured dendrites; blue asterisks: injury sites. Scale bars, 25 μm (A-A", D-D") and 10 μm (F-G"). For all quantifications, *p≤0.05, **p≤0.01, ***p≤0.001; n.s., not significant. The significance level above each genotype is for comparison with the control. Black bar, mean; red bar, SD. See also Figure S4.

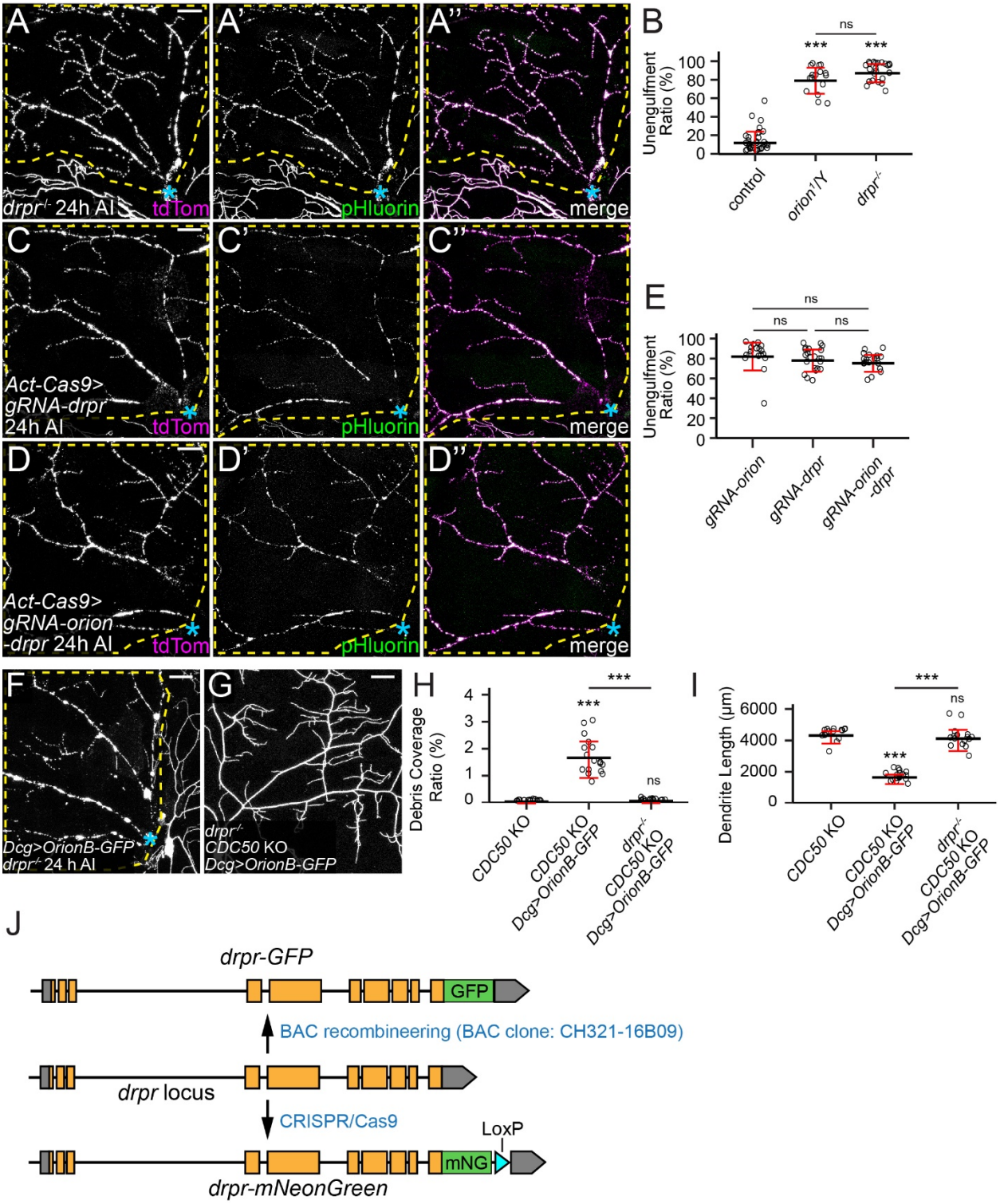

Figure S4: Orion recruits epidermal Drpr to injured dendrites

(A-A") Partial dendritic fields of a ddaC neuron in *drpr*$^{-/-}$ at 24 hrs AI.

(B) Quantification of unengulfment ratio of injured dendrites. n = number of neurons and N = number of animals: control and *orion*^{1}/Y (same dataset as in Figure 1D); *drpr*$^{-/-}$ (n = 23, N = 10). One-way ANOVA and Tukey's test.

(C-D") Partial dendritic fields of ddaC neurons at 24 hrs AI with whole-body *drpr* KO (C-C"), and *drpr+orion* double KO (D-D").

832 (E) Quantification of unengulfment ratio of injured dendrites. n = number of neurons and N = number of animals:
833 *orion* KO (same dataset as in Figure 2L); *drpr* KO (n = 23, N = 12); *orion*+*drpr* double KO (n = 19, N = 10). One-
834 way ANOVA and Tukey's test.
835 (F) Partial dendritic fields of an injured ddaC neuron with OrionB-GFP OE in fat body in the *drpr*$^{-/-}$ background at
836 24 hrs AI.
837 (G) Partial dendritic fields of a *CDC50* KO neuron with OrionB-GFP OE in fat body in the *drpr*$^{-/-}$ background.
838 (H-I) Quantification of debris coverage ratio (H) and dendrite length (I). n = number of neurons and N = number of
839 animals: *CDC50* KO and *CDC50* KO + *Dcg>OrionB-GFP* (96 hrs AEL, same dataset as in Figure 3K); *drpr*$^{-/-}$ +
840 *CDC50* KO + *Dcg>OrionB-GFP* (120 hrs AEL, n = 16, N = 8). For (H), Kruskal-Wallis (One-way ANOVA on
841 ranks) and Dunn's test, p-values adjusted with the Benjamini-Hochberg method; for (I), one-way ANOVA and
842 Tukey's test; ***$p \leq 0.001$; n.s., not significant. The significance level above each genotype is for comparison with
843 the control. Black bar, mean; red bars, SD.
844 (J) Schematic representation of Drpr-GFP and Drpr-mNG. Yellow boxes indicate exons, grey boxes indicate
845 untranslated regions.
846 Neurons were labeled by *ppk-MApHS* (A-A", C-D"), and *ppk-CD4-tdTom* (F-G). Scale bars, 25 μm.

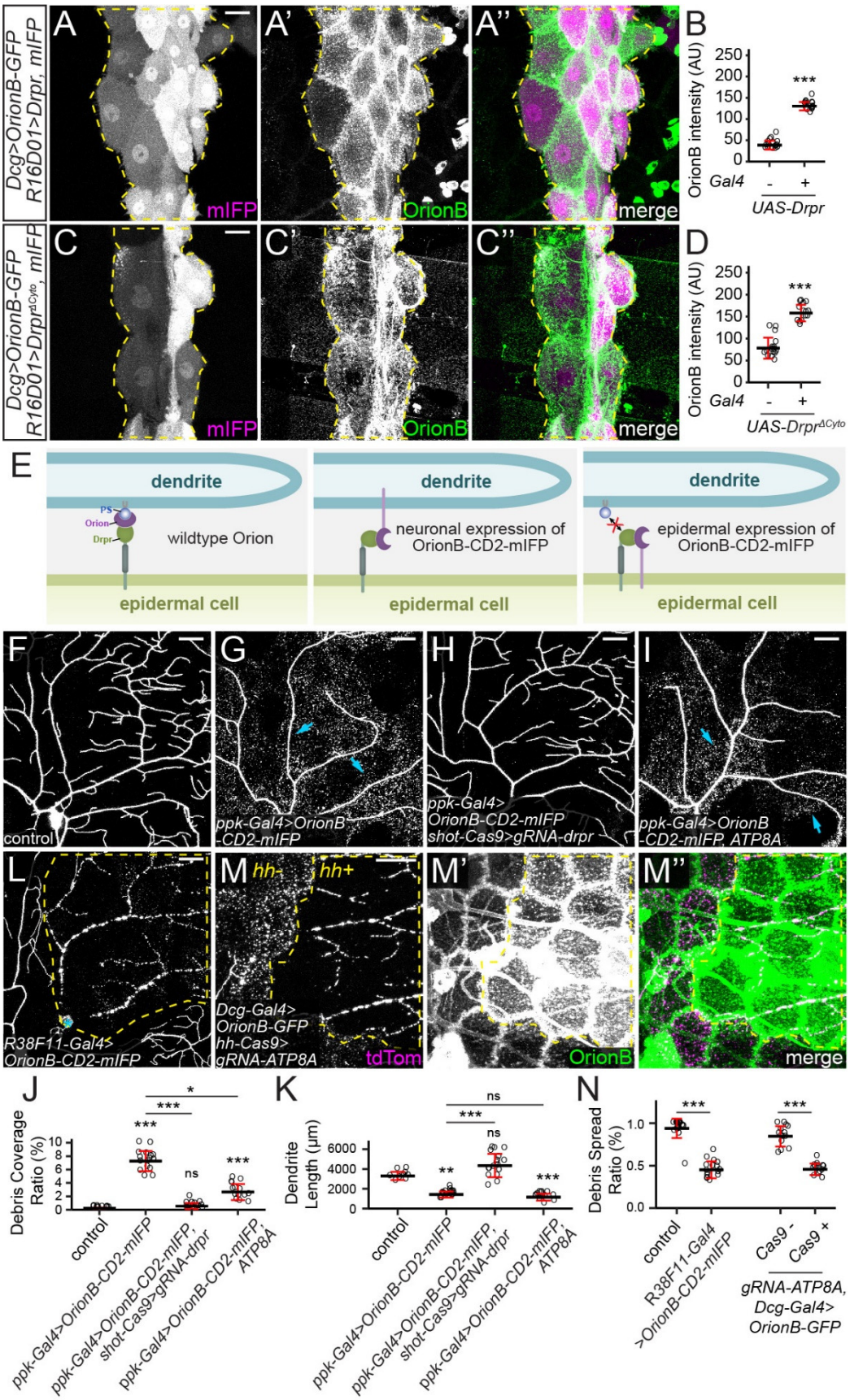
Dcg>OrionB-GFP
R16D01>Drpr, mIFP
A
A'
A''
mIFP
OrionB
merge
B
OrionB intensity (AU)
250
200
150
100
50
0
***
Gal4
-
+
UAS-Drpr
Dcg>OrionB-GFP
R16D01>Drpr^ΔCyto, mIFP
C
C'
C''
D
UAS-Drpr^ΔCyto
E
dendrite
PS
Orion
Drpr
wildtype Orion
neuronal expression of
OrionB-CD2-mIFP
epidermal expression of
OrionB-CD2-mIFP
epidermal cell
F
G
H
I
control
ppk-Gal4>OrionB
-CD2-mIFP
ppk-Gal4>
OrionB-CD2-mIFP
shot-Cas9>gRNA-drpr
ppk-Gal4>OrionB
-CD2-mIFP, ATP8A
L
M
M'
M''
hh-
hh+
R38F11-Gal4>
OrionB-CD2-mIFP
Dcg-Gal4>
OrionB-GFP
hh-Cas9>
gRNA-ATP8A
tdTom
OrionB
merge
J
Debris Coverage
Ratio (%)
10
8
6
4
2
0
*
***
ns
control
ppk-Gal4>OrionB-CD2-mIFP
ppk-Gal4>OrionB-CD2-mIFP,
shot-Cas9>gRNA-drpr
ppk-Gal4>OrionB-CD2-mIFP,
ATP8A
K
Dendrite
Length (μm)
6000
4000
2000
0
ns
**
N
Debris Spread
Ratio (%)
1.0
0.5
0.0
Cas9 -
Cas9 +
R38F11-Gal4
>OrionB-CD2-mIFP
gRNA-ATP8A,
Dcg-Gal4>
OrionB-GFP

847

848 **Figure 5: Orion mediates the interaction between PS and Drpr**
849 (A-A") Distribution of fat body-derived OrionB-GFP with Drpr overexpressed in a patch of epidermal cells driven
850 by R16D01-Gal4. mIFP was coexpressed with Drpr and thus the mIFP intensity is correlated with the Gal4 activity.
851 Yellow dash outlines: Drpr OE region.
852 (B) Quantification of Orion-GFP binding on epidermal cells with or without Drpr OE. n = number of measurements
853 and N = number of animals: without Drpr OE (n = 16, N = 8); with Drpr OE (n = 16, N = 8). Welch's t-test.
854 (C) Distribution of fat body-drived OrionB-GFP with $Drpr^{\Delta Cyto}$ overexpressed in a patch of epidermal cells (labeled
855 by mIFP). Yellow dash outlines: $Drpr^{\Delta Cyto}$ OE region.
856 (D) Quantification of Orion-GFP binding on epidermal cells with or without $Drpr^{\Delta Cyto}$ OE. n = number of
857 measurements and N = number of animals: without $Drpr^{\Delta Cyto}$ OE (n = 16, N = 8); with $Drpr^{\Delta Cyto}$ OE (n = 14, N = 7).
858 Welch's t-test.
859 (E) Models of Orion function in mediating PS-Drpr interaction (left), interactions between Drpr and Orion-CD2-
860 mIFP overexpressed by neurons (middle) or epidermal cells (right).
861 (F-I) Partial dendritic fields of a control ddaC neuron (F), an OroinB-CD2-mIFP OE neuron (G), an OroinB-CD2-
862 mIFP OE neuron with *drpr* KO in epidermal cells (H), and an OroinB-CD2-mIFP + ATP8A OE neuron (I).
863 (J-K) Quantification of debris coverage ratio (J) and dendrite length (K) at 96 hrs AEL. n = number of neurons and
864 N = number of animals: control (n = 10, N = 6); *ppk-Gal4>OroinB-CD2-mIFP* (n = 17, N = 9); *ppk-Gal4>OroinB-*
865 *CD2-mIFP + shot-Cas9>gRNA-drpr* (n = 17, N = 9); *ppk-Gal4>OroinB-CD2*-mIFP, *ATP8A* (n = 14, N = 7).
866 Kruskal-Wallis (One-way ANOVA on ranks) and Dunn's test, p-values adjusted with the Benjamini-Hochberg
867 method.
868 (L) Partial dendritic field of an injured ddaC neuron at 25 hrs AI with OroinB-CD2-mIFP expressed in all epidermal
869 cells.
870 (M-M") Partial dendritic field of an injured ddaC neuron at 9 hrs AI when OroinB-GFP was expressed in fat body
871 and *ATP8A* was knocked out in *hh*-epidermal cells.
872 (N) Quantification of debris spread index of injured dendrites. n = number of neurons and N = number of animals:
873 control (n = 18, N = 10); *R38F11>OroinB-CD2-mIFP* (n = 16, N = 8); *Dcg-Gal4>OrionB* (n = 14, N = 8); *Dcg-*
874 *Gal4>OrionB + hh-Cas9>ATP8A* (n = 13, N = 8). Welch's t-test.
875 Neurons were labeled by *ppk-MApHS* (F-I), and *ppk-CD4-tdTom* (L and M-M"). For all image panels, scale bars, 25
876 μm. For all quantifications, *p≤0.05, **p≤0.01, ***p≤0.001; n.s., not significant. The significance level above each
877 genotype is for comparison with the control. Black bar, mean; red bar, SD. See also Figure S5.
878
879
880
881
882

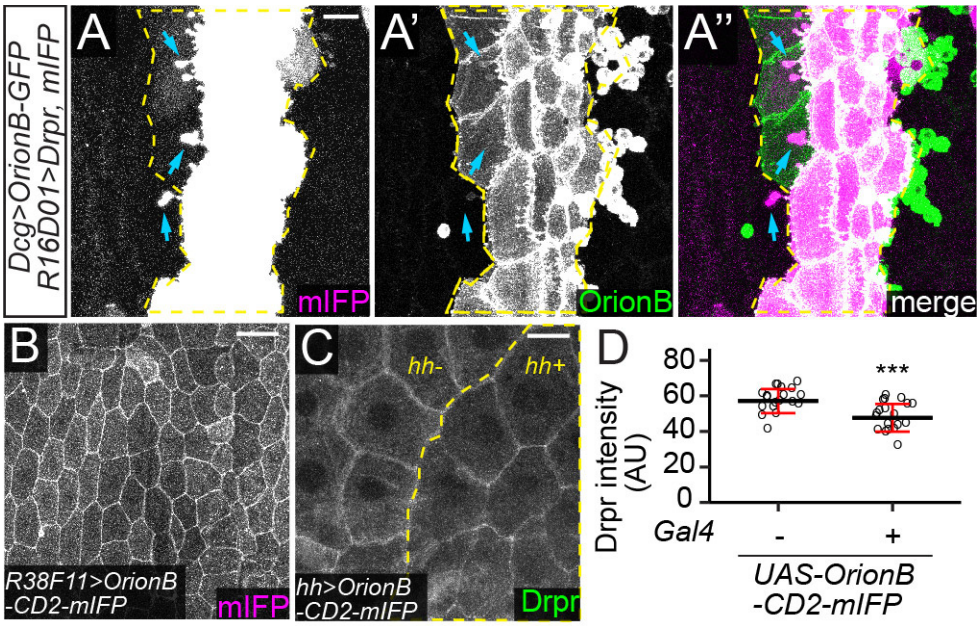

Figure S5: Orion mediates the interaction between PS and Drpr

(A-A") Protrusions (blue arrows) extended from Drpr OE epidermal cells (labeled by mIFP) in the presence of fat body-derived OrionB-GFP. Yellow dash outlines: Drpr OE region.

(B) OrionB-CD2-mIFP localization in epidermal cells driven by *R38F11-Gal4*.

(C) Drpr localization in epidermal cells with OrionB-CD2-mIFP expressed in the *hh* domain. Yellow dash outlines: *hh-Gal4>OrionB-CD2-mIFP* region.

(D) Quantification of stained Drpr levels in epidermal cells with or without OrionB-CD2-mIFP OE. n = number of measurements: w/o OrionB-CD2-mIFP OE (n = 19); w/ OrionB-CD2-mIFP OE (n = 19). Welch's t-test; ***$p \leq 0.001$; black bar, mean; red bars, SD.

Scale bars, 25 µm (A-A" and C), 50 µm (B).

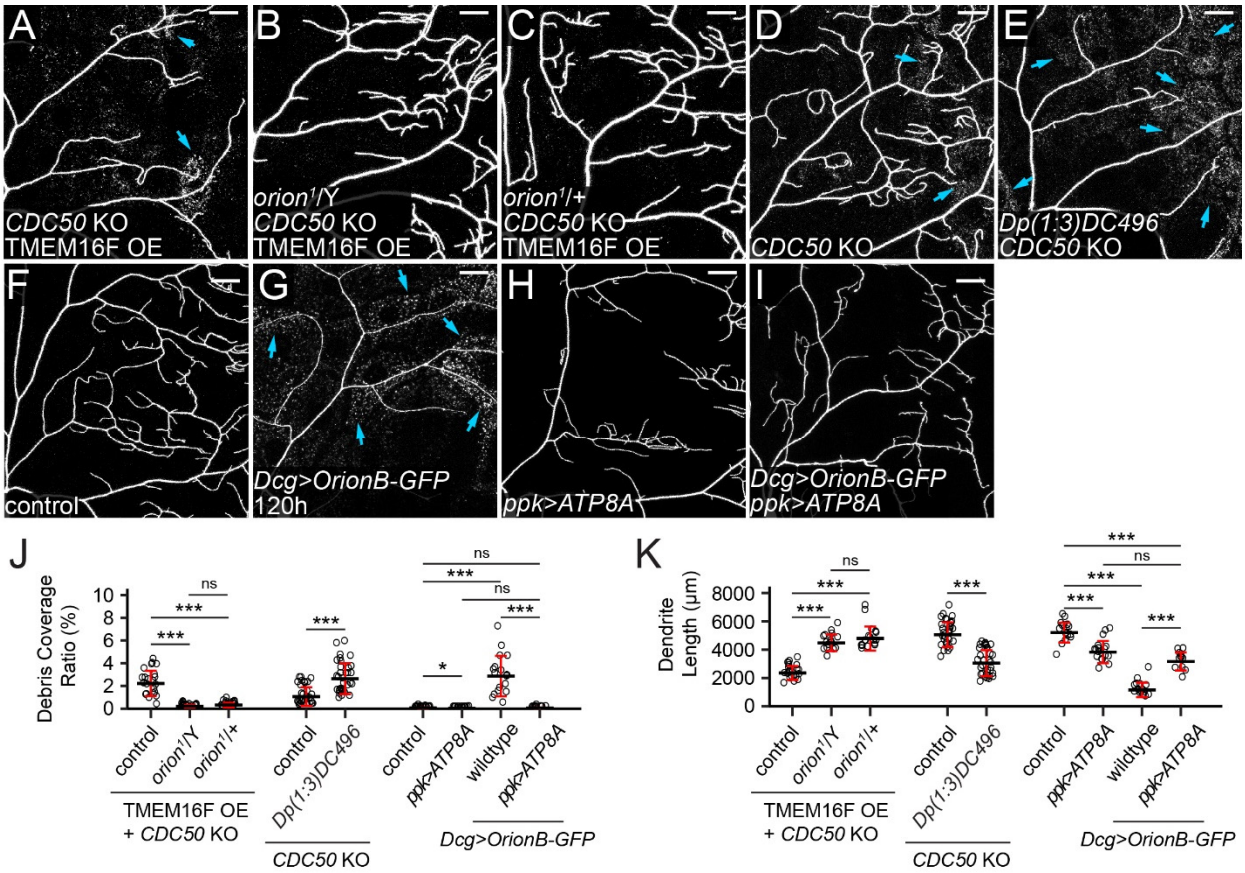

Figure 6: The Orion dosage determines the sensitivity of epidermal cells to PS-exposing dendrites

(A-C) Partial dendritic fields of a TMEM16F OE + *CDC50* KO ddaC neuron in the WT background (A, same image as Figure 1E), in the *orion*^{1} hemizygous background (B, same image as Figure 1F), and in the *orion*^{1} heterozygous background (C).

(D-E) Partial dendritic fields of *CDC50* KO neurons in the control (D) and Dp(1;3)DC496 (E) at 120 hrs AEL. Blue arrows: debris shed from dendrites.

(F-I) Partial dendritic fields of ddaC neurons in the control (F), with fat body-derived OrionB-GFP (G), with ATP8A OE in the neuron (H), and with fat body-derived OrionB-GFP and ATP8A OE in the neuron (I) at 120 hrs AEL.

(J-K) Quantification of debris coverage ratio (J) and dendrite length (K). n = number of neurons and N = number of animals: for TMEM16F OE + *CDC50* KO, control and *orion*^{1}/Y (same dataset as in Figure 1G), *orion*^{1}/+ (n = 18, N = 9); for (J), Kruskal-Wallis (One-way ANOVA on ranks) and Dunn's test, p-values adjusted with the Benjamini-Hochberg method; for (K), one-way ANOVA and Tukey's test. For *CDC50* KO, control (n = 33, N = 17), Dp(1;3)DC496 (n = 33, N = 17), Welch's t-test. For effects of *Dcg>OrionB-GFP* and *ppk>ATP8A* at 120 hrs AEL, control (n = 17, N = 9), *ppk>ATP8A* (n = 17, N = 9), *Dcg>OrionB-GFP* (n = 17, N = 9), *ppk>ATP8A* + *Dcg>OrionB-GFP* (n = 12, N = 7); for (J), Kruskal-Wallis (One-way ANOVA on ranks) and Dunn's test, p-values adjusted with the Benjamini-Hochberg method; for (K), one-way ANOVA and Tukey's test.

Neurons were labeled by *ppk-MApHS* (A-C and H), *ppk-CD4-tdTom* (D-G), and *ppk-Gal4>CD4-tdTom* (I). For all image panels, scale bars, 25 µm. For all quantifications, *p≤0.05, ***p≤0.001; n.s., not significant. The significance level above each genotype is for comparison with the control. Black bar, mean; red bars, SD. See also Figure S6.

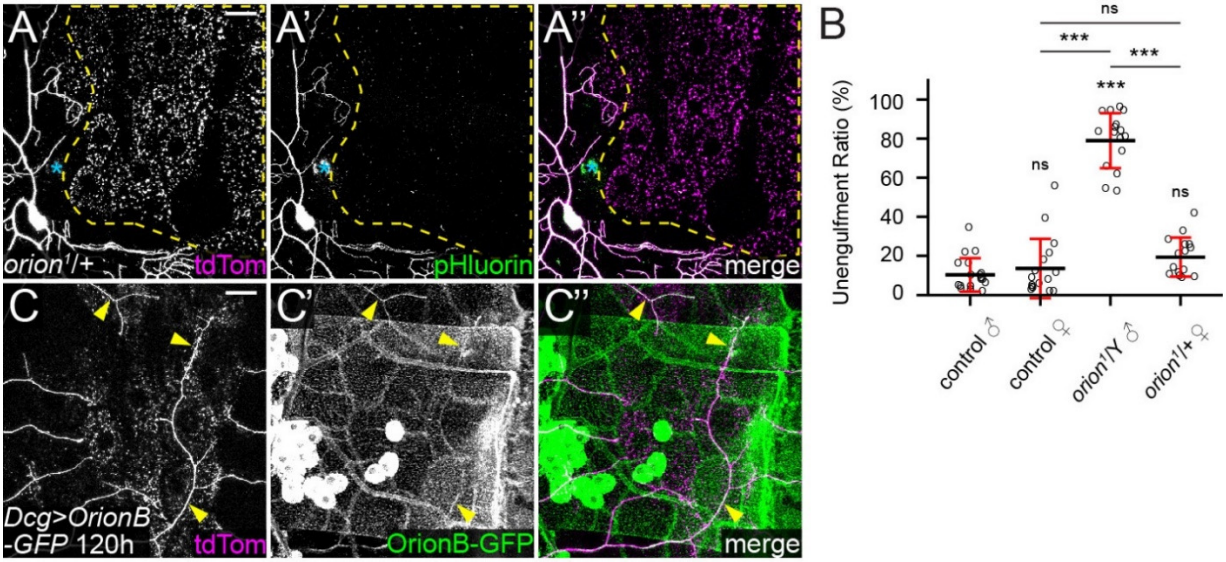

Figure S6: The Orion dosage determines the sensitivity of epidermal cells to PS-exposing dendrites

(A-A") Partial dendritic fields of a ddaC neuron in an *orion*^{1} heterozygous larva at 22 hrs AI. Yellow dash outlines: territories originally covered by injured dendrites; blue asterisks: injury sites.

(B) Quantification of unengulfment ratio of injured dendrites. n = number of neurons and N = number of animals: control males, control females, and *orion*^{1}/Y (same dataset as in Figure 1D); *orion*^{1}/+ (n = 15, N = 8). One-way ANOVA and Tukey's test; ***$p \leq 0.001$; n.s., not significant. The significance level above each genotype is for comparison with the control. Black bar, mean; red bars, SD.

(C-C") Partial dendritic fields of a wildtype neuron with OrionB-GFP OE in the fat body at 120 hrs AEL. Yellow arrowheads: OrionB-GFP colocalizing with dendrites.

Neurons were labeled by *ppk-MApHS* (A-A"), and *ppk-CD4-tdTom* (C-C"). For all image panels, scale bars, 25 µm.

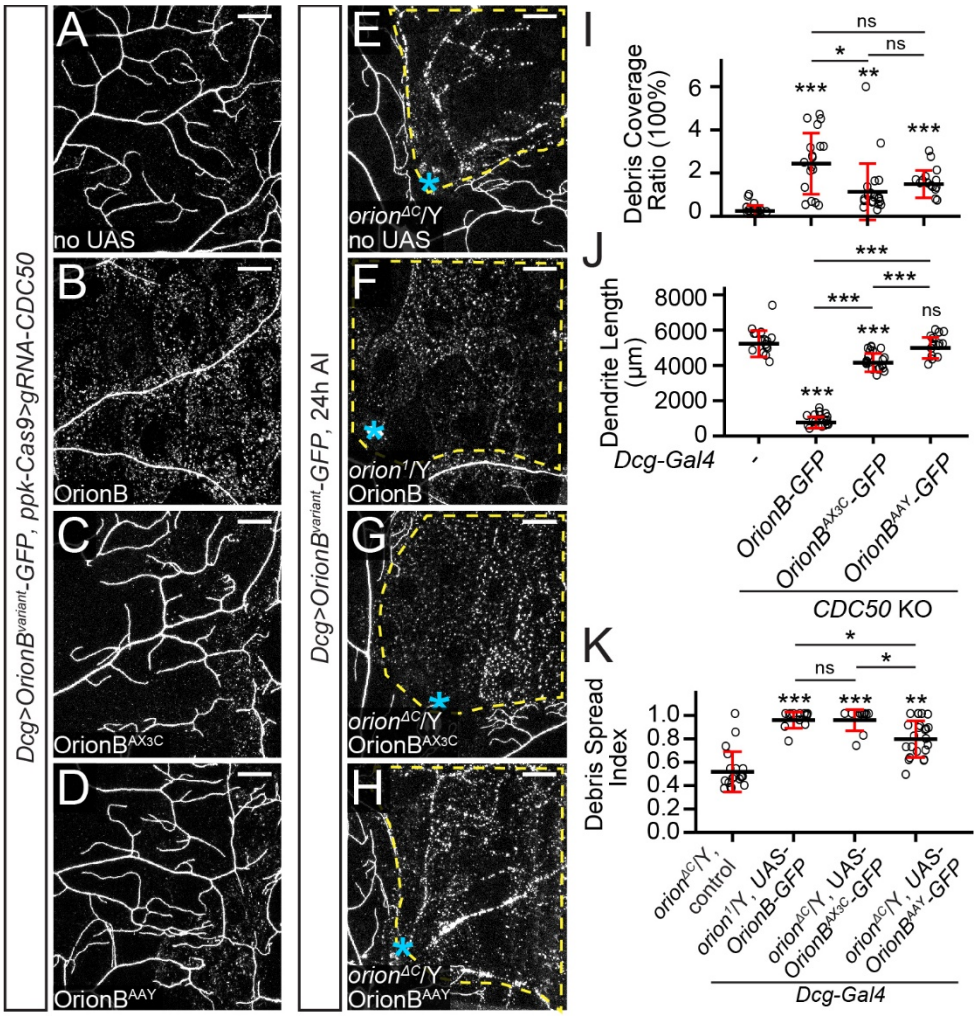

Figure 7: CX_3C and RRY motifs are important for Orion function

(A-D) Partial dendritic fields of *CDC5O* KO ddaC neurons without OrionB variants (A), with WT OrionB=GFP (B), OrionB^{AX3C}-GFP (C), and OrionB^{AAY}-GFP (D) expressed in the fat body at 120 hrs AEL.

(I-J) Quantification of debris coverage ratio (I) and dendrite length (J) at 120 hrs AEL. n = number of neurons and N = number of animals: *CDC50* KO control (n = 16, N = 8); *CDC50* KO + *Dcg>OrionB-GFP* (n = 18, N = 9); *CDC50* KO + *Dcg>OrionB^{AX3C}-GFP* (n = 20, N = 10); *CDC50* KO + *Dcg>OrionB^{AAY}-GFP* (n = 16, N = 8); *CDC50* KO + *Dcg>OrionB^{1}-GFP* (n = 15, N = 8). For (I), Kruskal-Wallis (One-way ANOVA on ranks) and Dunn's test, p-values adjusted with the Benjamini-Hochberg method; for (J), one-way ANOVA and Tukey's test.

(E-H) Partial dendritic fields of ddaC neurons in *orion$^{\Delta C}$* or *orion^{1}* hemizygous larvae without OrionB variants (E), with WT OrionB=GFP (F), OrionB^{AX3C}-GFP (G), and OrionB^{AAY}-GFP (H) expressed in the fat body at 22-24 hrs AI. Yellow dash outlines: territories originally covered by injured dendrites; blue asterisks: injury sites.

(K) Quantification of debris spread index of injured dendrites. n = number of neurons and N = number of animals: *orion$^{\Delta C}$*/Y control (n = 19, N = 9); *orion^{1}*/Y + *Dcg>OrionB-GFP* (same dataset as in 2M); *orion$^{\Delta C}$*/Y + *Dcg>OrionB^{AX3C}-GFP* (n = 12, N = 7); *orion$^{\Delta C}$*/Y + *Dcg>OrionB^{AAY}-GFP* (n = 23, N = 12); *orion$^{\Delta C}$*/Y + *Dcg>OrionB^{1}-GFP* (n = 15, N = 8). Kruskal-Wallis (One-way ANOVA on ranks) and Dunn's test, p-values adjusted with the Benjamini-Hochberg method.

For all image panels, neurons were labeled by *ppk-CD4-tdTom*. Scale bars, 25 µm. For all quantifications, *p≤0.05, **p≤0.01, ***p≤0.001; n.s., not significant. The significance level above each genotype is for comparison with the control. Black bar, mean; red bars, SD.